AD-A075 506 NAVAL RESEARCH LAB WASHINGTON DC F/G 11/6
FATIGUE CRACK GROWTH OF A508 STEEL IN HIGH-TEMPERATURE, PRESSUR--ETC(U)
SEP 79 W H CULLEN, V PROVENZANO
UNCLASSIFIED NRL-MR-4063 NL

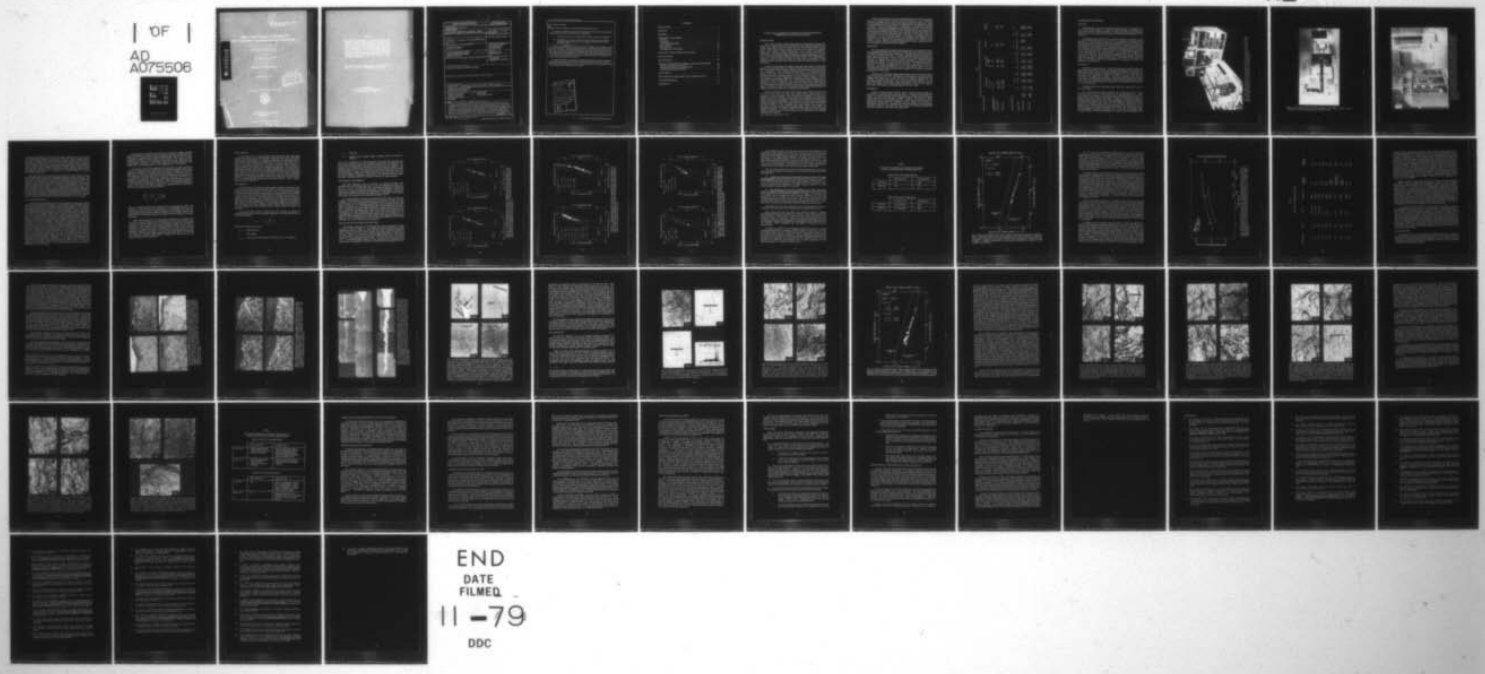

END
DATE FILMED
11-79
DDC

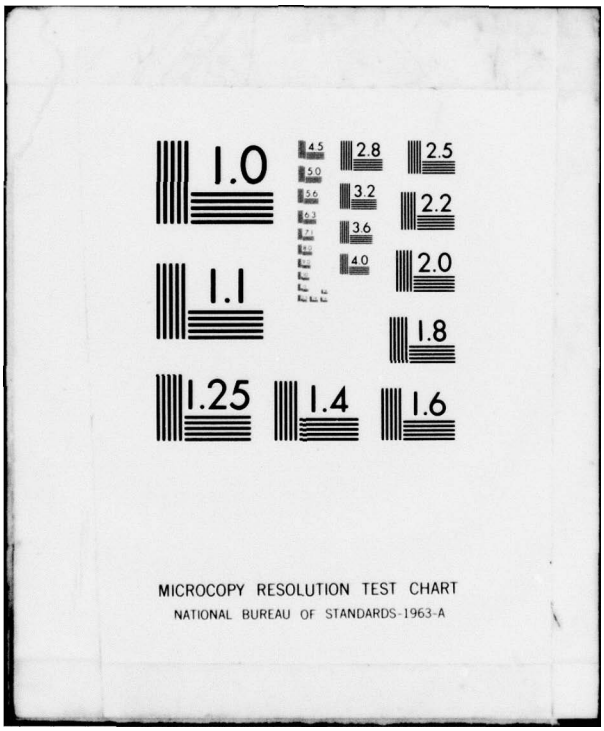
1.0
1.1
1.25
1.4
1.6
1.8
2.0
2.2
2.5
2.8
3.2
3.6
4.0
4.5
5.0
5.6
6.3
7.1
MICROCOPY RESOLUTION TEST CHART
NATIONAL BUREAU OF STANDARDS-1963-A

(14) NRL-MR-4063
NRL/NUREG-CR-0969

SECURITY CLASSIFICATION OF THIS PAGE (When Data Entered)

REPORT DOCUMENTATION PAGE

READ INSTRUCTIONS BEFORE COMPLETING FORM

1. REPORT NUMBER: NRL Memorandum Report 4063
NUREG/CR 0969

2. GOVT ACCESSION NO.

3. RECIPIENT'S CATALOG NUMBER

4. TITLE (and Subtitle) (6)
FATIGUE CRACK GROWTH OF A508 STEEL IN HIGH-TEMPERATURE, PRESSURIZED REACTOR-GRADE WATER

5. TYPE OF REPORT & PERIOD COVERED
Interim report on a continuing NRL problem.

6. PERFORMING ORG. REPORT NUMBER

7. AUTHOR(s) (10)
W. H. Cullen, Jr., V. Provenzano, K. J. Torronen*, H. E. Watson and F. J. Loss

8. CONTRACT OR GRANT NUMBER(s)

9. PERFORMING ORGANIZATION NAME AND ADDRESS
Naval Research Laboratory
Washington, DC 20375

10. PROGRAM ELEMENT, PROJECT, TASK AREA & WORK UNIT NUMBERS
NRL Problem M01-40
Project ~~RES-79-103~~

11. CONTROLLING OFFICE NAME AND ADDRESS (12) 58
U.S. Nuclear Regulatory Commission
Division of Reactor Safety Research
Washington, DC 20555

12. REPORT DATE
September 28, 1979

13. NUMBER OF PAGES
56

14. MONITORING AGENCY NAME & ADDRESS(if different from Controlling Office) (11) 28 Sep 79

15. SECURITY CLASS. (of this report)
UNCLASSIFIED

15a. DECLASSIFICATION/DOWNGRADING SCHEDULE

16. DISTRIBUTION STATEMENT (of this Report)
Approved for public release; distribution unlimited.

NRL-MR-4063

17. DISTRIBUTION STATEMENT (of the abstract entered in Block 20, if different from Report)

18. SUPPLEMENTARY NOTES
*Present address: Technical Research Centre of Finland, 02150 ESPOO 15, Finland
Prepared for the U.S. Nuclear Regulatory Commission, Office of Nuclear Regulatory Research under Interagency Agreement ~~RES-79-103~~.
NRC Distribution Category R5

19. KEY WORDS (Continue on reverse side if necessary and identify by block number)
Fatigue crack propagation
Hydrogen embrittlement
Nuclear pressure vessel steel
Fractography
Metallography
Stress-corrosion cracking

degree

20. ABSTRACT (Continue on reverse side if necessary and identify by block number)
Fatigue crack growth tests of A508-2 pressure vessel steel have been conducted at two test temperatures (93°C and 288°C) using a variety of constant amplitude waveforms. The load ratios were either 0.1 or 0.125, and the water chemistry was carefully monitored and controlled so as to simulate the nominal pressurized water reactor chemistry. The test procedures are described, and an examination of all the data indicates that the results fall into one of two rather clearly defined categories. One band of data, termed "low", lies close to or essentially on, the ASME Section XI Code air environment default line. The other band of data, termed "high", resides approximately

(Continues)

DD FORM 1 JAN 73 1473 EDITION OF 1 NOV 65 IS OBSOLETE
S/N 0102-014-6601

SECURITY CLASSIFICATION OF THIS PAGE (When Data Entered)

251 950

JOB

20. Abstract (Continued)

midway between the ASME Sec. XI air and water environment default lines.

The two bands of data are the result of certain combinations of the waveform and temperature variables listed above, and are determined by the following rules:

(1) a ramp time in excess of one second is needed to obtain the high crack growth rate;

(2) the application of a hold time, together with a high temperature, serves to depress a normally high crack growth rate test (i.e. one with a long ramp time) and force it into the low category.

A hydrogen embrittlement model is used as a basis for the explanation of this behavior. During the longer ramp times (~ one second) hydrogen, formed by aqueous hydrolysis, diffuses into the plastic zone, resulting in local embrittlement. However, if the test involves a waveform with a hold time component, and a high temperature, the hydrogen diffuses out of the plastic enclave and the crack growth rates are not accelerated from the "low" to the "high" category. Short ramp times (~ one second) at either temperature, do not allow a significant production of hydrogen ions, and the growth rates remain in the "low" category.

The suggested mechanism is supported by fractographic observations of increased intergranular and quasi-cleavage components for the hydrogen assisted fatigue crack growth modes, while the fatigue fracture surfaces of specimens from the low growth rate category showed a higher percentage of striation formation and transgranular growth modes.

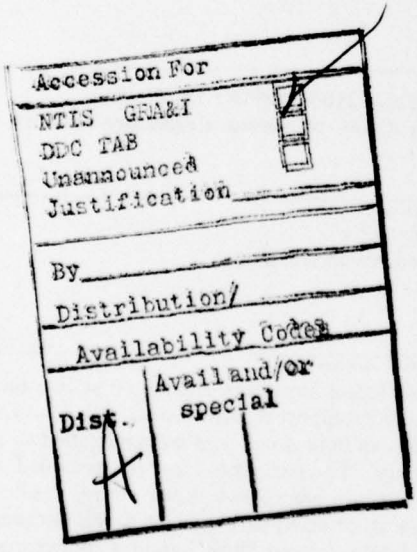

CONTENTS

FATIGUE CRACK GROWTH OF A508 STEEL IN HIGH-TEMPERATURE PRESSURIZED REACTOR GRADE WATER

INTRODUCTION

The American Society of Mechanical Engineers (ASME) Boiler and Pressure Vessel Code - Section XI contains information on the fatigue crack growth rate (da/dN) upper limits allowed in certain nuclear reactor safety-related computations. These upper limits are given in the form of two da/dN vs ΔK (applied cyclic stress intensity factor) relationships. One of these relationships is appropriate to the case of fatigue crack growth in an air environment, the other to the case of the high-temperature pressurized reactor grade water environment. In the safety analysis of Section XI, these da/dN vs ΔK relationships are employed in lieu of actual data from the steels used in construction of that particular reactor pressure vessel (RPV) for which the safety analysis is being carried out.

In order to investigate the validity and conservative nature of the ASME Section XI procedures, research is being conducted to show that commonly used RPV steels do not exhibit corrosion fatigue crack growth rates which exceed the Sec. XI guidelines. This involves performing tests in an environment which models that of the primary coolant in the nuclear systems, using materials produced according to accepted practice for the nuclear industry. To address this concern, the Nuclear Regulatory Commission (NRC), together with the Naval Research Laboratory (NRL) and Westinghouse Nuclear Energy Systems developed in 1976 a preliminary test matrix, setting down combinations of waveforms and test temperatures which have now been tested. Data obtained from this program was used to develop a second test matrix encompassing a wide range of materials but only the two waveforms which consistently produced the highest crack growth rates of the preliminary matrix results.

One of the intents of the preliminary matrix was to delineate the effects of rise time and hold time within the loading pattern, and therefore, the waveforms of the preliminary matrix scheme were composed of ramp times ranging from one sec. to thirty min. and hold times ranging from essentially zero (reset) to sixty min. Additionally a one cycle per min. sinewave test was run to support the proposed conclusions. For all tests at the NRL, the load ratio was either 0.1 or 0.125. The two test temperatures of the matrix were 93°C (200°F) and 288°C (550°F). These selections were made because they spanned the characteristics expected during the heatup/cooldown cycle and the hydro- and leak-test transients. To provide uniformity to the results, the same material (A508-2) was used in all of these tests, and the environment was carefully monitored and regulated.

Note: Manuscript submitted August 7, 1979.

While the crack growth rate data were being developed, post-test examination of the fatigue fracture surfaces yielded information on the mechanistic processes responsible for the growth rate behavior which was observed. Toward the concluding months of the study, as the significance of the observations began to cohere, a more intensified effort to understand the mechanistic processes resulted in a redoubled metallographic and fractographic effort. The end result is this report, containing descriptions of the techniques used in high-temperature pressurized water fatigue crack growth rate testing, a large volume of data, and some observations on the characteristics of that data. These observations are supported by a model involving hydrogen embrittlement, including effects of temperature, rise time and hold time on the hydrogen specie behavior. This model is in turn supported by fractographic observations on selected fatigue fracture surfaces which demonstrate fractographic features characteristic of known hydrogen embrittlement assisted failure.

APPROACH

The environmental and fatigue loading parameters were selected to simulate operating pressurized water reactors. In these systems, the primary coolant is derived from high purity water containing 1000 ppm boron as boric acid and 1 ppm lithium as lithium hydroxide. All other elemental contaminent species are held to less than 0.15 ppm. In these test systems, the reactor environment was simulated by adding boric acid and lithium hydroxide to deionized water. Typically, the analysis of the water, performed once weekly, showed: boron -1000 ppm $\pm$50 ppm, lithium - 1.00 ppm $\pm$0.05 ppm, chlorine - 0.50 ppm and fluorine - 0.2 ppm. The specific conductance of this reactor-grade water is 16 to 20 μmhos/cm and the pH approaches 5.8 from an initial value of about 6.7 to 6.8. The dissolved oxygen level is held as low as possible (0 to 2 ppb) by continuous deoxygenation of the water.

Nearly all of the fatigue loading cycles employed were composed of linear ramp, a hold period, and a reset. Individually these components may have periods ranging from nearly zero to one hour and are chosen to approximate the timewise fluctuations of pressure and stress in an operating reactor. In the concluding stages of this study, 1 cpm sine waveforms were added to the test plan. For the purposes of this test series, load ratios of 0.1 to 0.2 were chosen. Extensions of this study are employing load ratios of 0.7 as well.

MATERIALS

A508 is a low alloy steel commonly used by American reactor vendors for construction of nuclear reactor pressure vessels. Complete specifications are found in the ASTM Standard A508-77-Quenched and Tempered Vacuum-Treated Carbon and Alloy Steel Forgings for Pressure Vessels. Two heats of A508-2 forging material were used in this research. In both cases, the specimens were taken from nozzle drop-outs furnished to NRL through the courtesy of Westinghouse Corporation. Chemical and mechanical properties of the materials are given in Table 1. The codes FW- and R- serve as materials identification codes and represent the two heats mentioned above.

Table 1

Mechanical and Chemical Properties of the Pressure Vessel Steels Used in this Study

Mechanical Properties

	Yield Strength MPa (ksi)	Ultimate Tensile Strength MPa (ksi)	Elongation %	Reduction Area
Current Requirements (A508-Class 2)	345 (50)	550 (80)	20	--
FW-specimens	456 (66.1)	617 (89.5)	26.5	69.4
	464 (67.3)	614 (89.1)	25.5	68.7
R-specimens	467 (67.8)	613 (89)	25.5	72.9
	455 (66.0)	600 (87)	25.5	74.1

Chemical Composition

		C	Mn	P	S	Si	Ni	Cr	V	Mo	Co
Requirements		0.27	0.5/1.0	0.025	0.025	0.15/0.4	0.5/1.0	0.25/0.45	0.05	0.55/0.7	
FW-Specimens	Ladle	0.23	0.58	0.009	0.010	0.24	0.70	0.33	0.02	0.61	0.010
	Checks	0.19	0.60	0.010	0.012	0.26	0.70	0.33	0.02	0.57	0.008
		0.21	0.60	0.010	0.011	0.27	0.69	0.33	0.02	0.56	0.008
R-Specimens	Ladle	0.20	0.64	0.006	0.009	0.23	0.69	0.38		0.59	0.01
	Checks	0.19	0.64	0.010	0.009	0.23	0.69	0.42		0.60	0.01
		0.20	0.65	0.010	0.007	0.23	0.68	0.40		0.60	0.01

EXPERIMENTAL PROCEDURE

Specimens

Specimens were cut from the nozzle drop-outs by first removing about 40 mm of the outside surface, including the inside cladding, and blanking out specimens from the remaining material. All specimens were oriented so that the tensile stress at the crack tip was parallel to the hoop stress direction of the drop-out.

The samples were either 25.4 mm thick (1T) compact specimens, or 50.8 mm thick (2T) WOL specimens. In the case of the compacts, the machined notch extended to an a/W of 0.25 and these were precracked to an a/W of 0.30. The WOL specimens had a machined notch 25.4 mm (a/W = 0.19) and were precracked an additional 6 to 50 mm (0.3 to 2 in.) depending on the initial ΔK level desired. The maximum stress intensity applied during precracking was less than or equal to the initial stress intensity levels for the test. All precracking was performed at room temperature in an air environment. At the time some of these tests were carried out, there was considerable speculation about the existence of a "starting ΔK" effect [1], hence the choice of initial precrack lengths in the WOL specimens spanning an unusually large range. The results of this particular aspect of the study, which do not substantiate the starting ΔK effect, are discussed in a later section.

Containment

These tests are performed in closed environmental chambers which are appropriately constructed for the environment, temperature and pressure regimes under study. The low-temperature tests (93°C, 200°F) were run in a small stainless steel vessel (called a "waterpot") holding about 6 ℓ of water (Fig. 1). The water was circulated at about 1 ℓ/hr and a nitrogen cover gas was maintained at a slightly positive pressure. Resistance strip heaters were welded to the sides of the waterpot and suitable control held the temperature to within +2°C. No on-line water analysis was available for this system at the time these tests were carried out.

The high temperature pressurized water tests were carried out in one of three autoclaves:

(a) A single specimen (1T-CT) autoclave, (b) a single specimen (2T or 4T) autoclave, Fig. 2, or (c) a multispecimen (1, 2 or 4T) autoclave, Fig. 3. While these devices are different in size and physical construction, they are similar in operation and can be described ensemble. Pressure is maintained in each by a Sprague piston pump which is set to pump continuously at about one stroke/sec. An overpressure release valve set at 13.7 MPa (2000 psi) maintains a constant pressure by releasing excess water from the system at each stroke of the Sprague pump. This pump-release valve combination thus circulates at a rate of about 10 ℓ per hour, as well as pressurizes the water. The water released from the high-pressure autoclave loop flows into a make-up or feedwater tank, spraying through a cover gas of hydrogen as it enters. This action assists in the

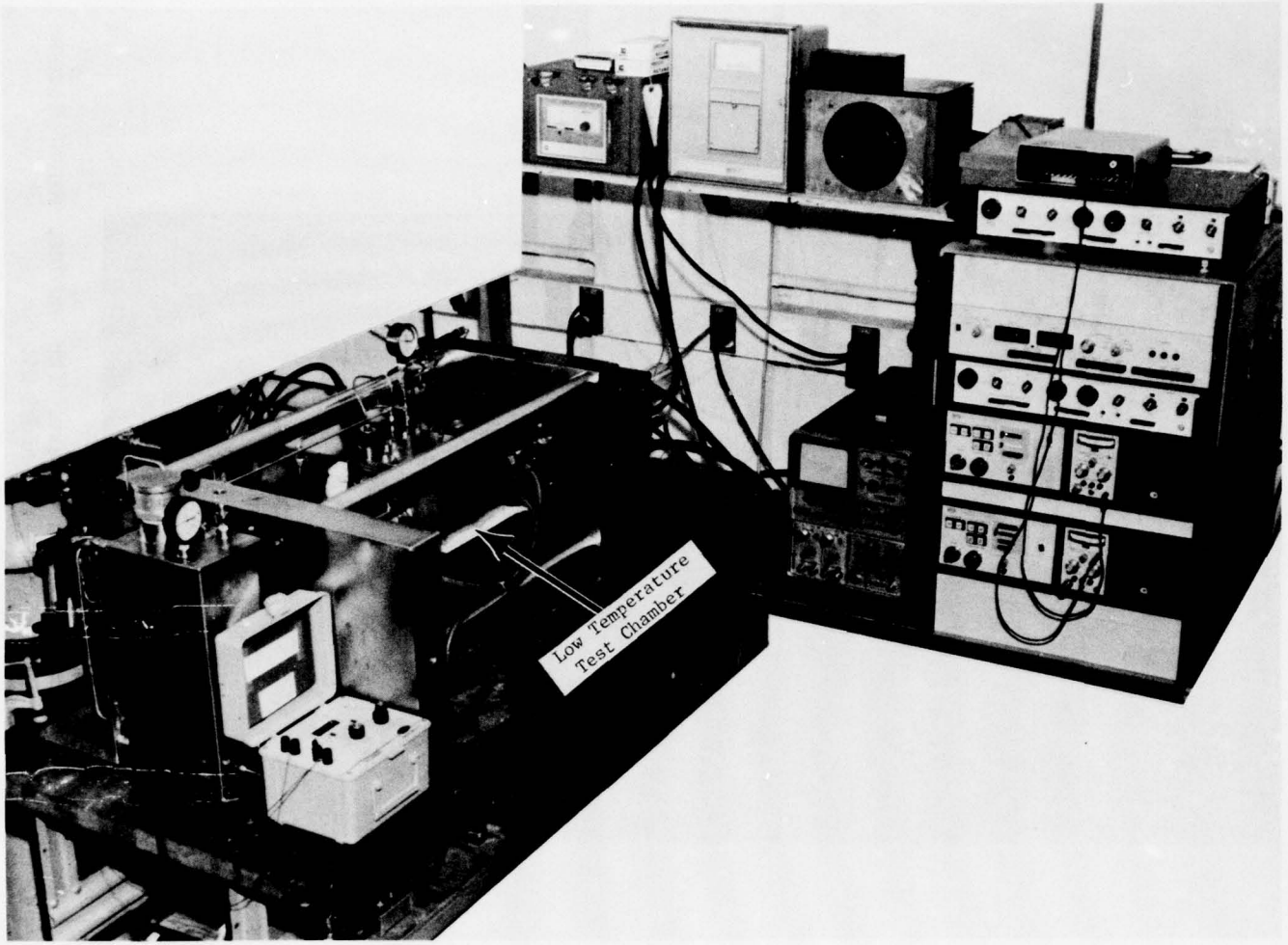

Fig. 1 The single specimen, low-temperature (93°C) water pot. This device was used for all of the 93°C tests of this study. Although it uses nitrogen as a cover gas, the oxygen levels are 1-2 ppb, the same as the autoclaves.

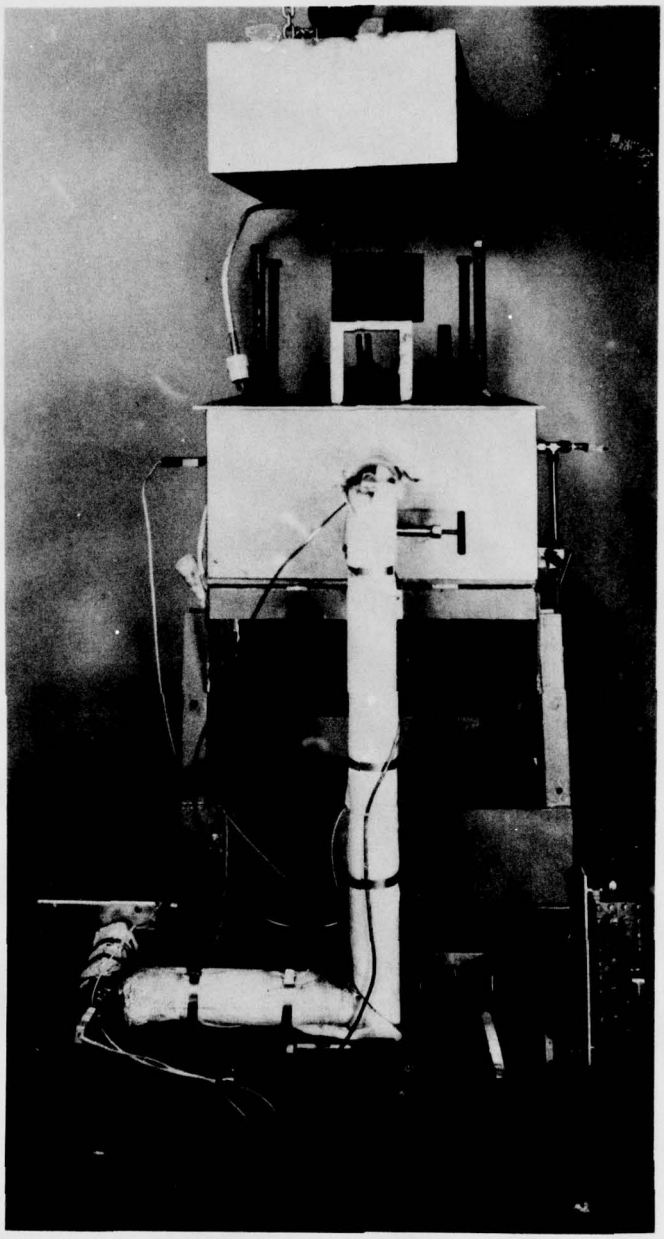

Fig. 2. The single specimen (2/4T) autoclave. This device, which became operational in late 1978, was used in the test of R2-05.

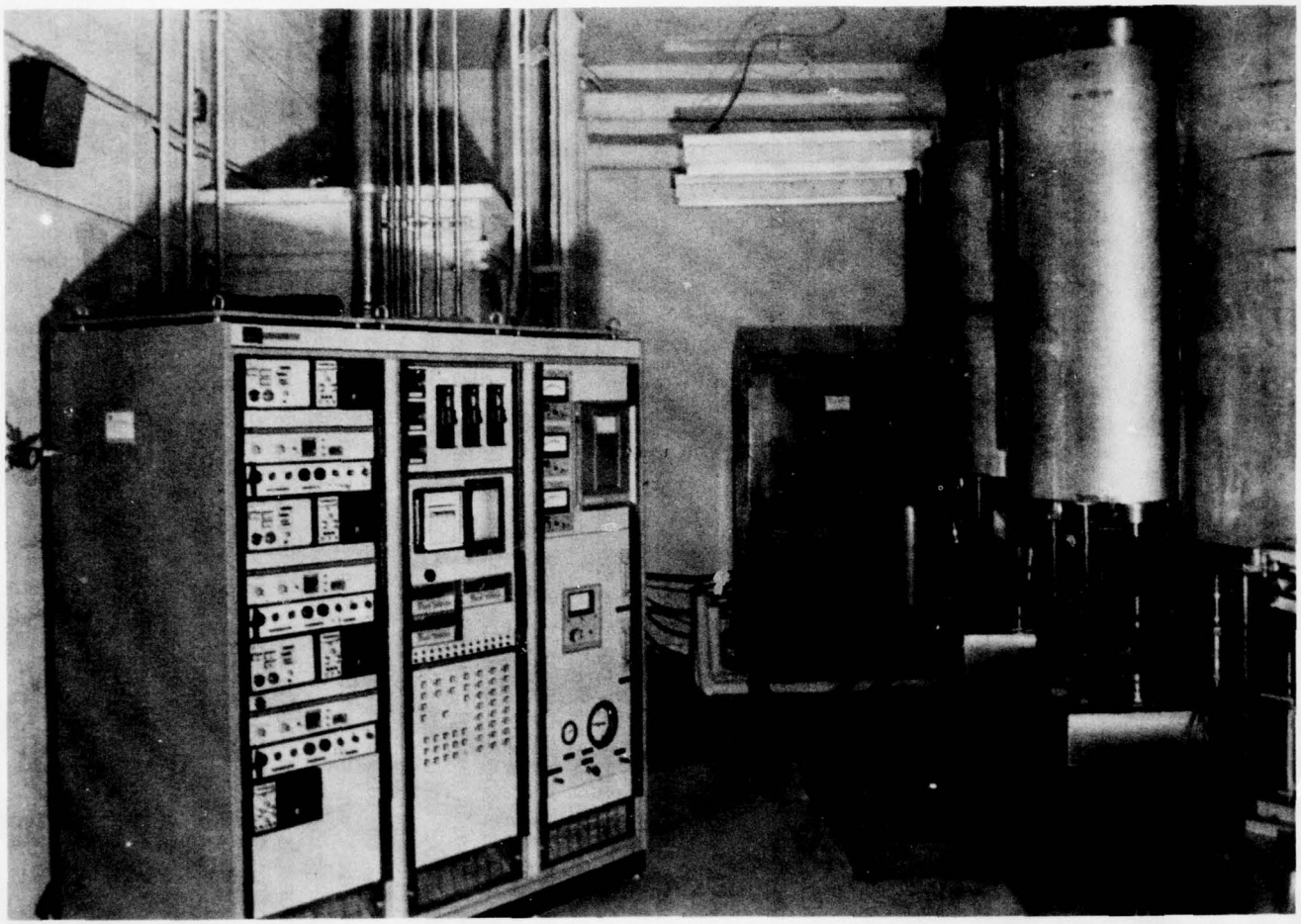

Fig. 3. The multispecimen autoclave facility. These devices, which became operational toward the close of this study, provided the data of specimens R2-11 and R2-12. Each chamber has independent hydraulic and temperature controls, and the load command signal is electronically compensated for changes in pressure.

continuous deoxygenation of the water and enables maintenance of the less than 1 to 2 ppb levels of oxygen in the systems. The on-line water analysis systems for specific conductivity and dissolved oxygen content, which, at the time of this study, were available only for the 2/4T and the multispecimen autoclaves, circulated water to and from the make-up tank through the electrode chambers for the various types of analysis available (dissolved oxygen, specific conductivity and pH). For each of the four systems, a batch sample of about one liter was drawn off each week for a complete wet chemical analysis for various metallic and halide ions.

The load rods into the chambers are sealed with either teflon or silicon rubber gaskets and the load loss is negligible compared to the applied load. The force of the water pressure on the load rod cross-sectional area is algebraically subtracted from the load as realized at the externally situated load cell. The waveforms are generated by function generators and the loads are applied using standard fatigue rated actuators in closed loop servohydraulic test frames. Every attempt is made to allow a test to proceed twenty-four hours a day, seven days a week from start to finish, however, interruptions for repairs, replacement of failed gaskets, etc. are occasionally necessary and are performed as rapidly as possible so as to alleviate transient phenomenon in the data generation. In spite of these efforts, transient accelerations and decelerations in the crack growth rate are observed and these will be indicated and discussed in a later section.

Crack Length Measurement

Because the crack extension cannot be continuously measured using optical means, this quantity was determined from an experimentally developed relationship between the specimen compliance and the crack length. In this case the compliance was defined as the ratio of crack mouth displacement (δ) to load (P). The displacement measurements were made using linear variable differential transformers (LVDT) gages, designed for use in this environment, and fastened to the mouth of the specimen using either a flexible cable attached to the core piece, or a trunnion mount, to assure the required rotational degree of freedom. Before the LVDT units are "baked-out" at temperatures about 10 % greater than operating temperature and cycled between ambient and operating temperatures several times to insure stability. Each LVDT is associated with a specific conditioner unit and is calibrated at operating temperature as well as room temperature prior to use. Calibration is performed using a dial micrometer to drive the corepiece while the body of the LVDT is held rigidly in a tube furnace. Readings of displacement and voltage output are taken at about twenty evenly-spaced intervals and the results computer fit to a straight line, the slope of which is the calibration coefficient. The gain, and mechanical and electrical zero points are appropriately adjusted to give as linear a response over the required displacement range as possible. It is found that the temperature dependence of the calibration coefficient is of the order of 10^{-5} V/^{o}C for the larger (12.7 mm, 0.500 in.) stroke LVDT units and about 2×10^{-6} V/^{o}C for the smaller (2.5 mm, 0.100 in.) units. We have not been able to discern any pressure dependence of the LVDT units.

Crack length to compliance relationships are produced by fatigue cracking (2T-WOL specimens) or using a series of specimens with varying machined notch lengths (1T-CT specimens) and measuring displacement/load (δ/P) as a function of optically measured surface crack or notch length. The results are then computer curve-fitted to an appropriate non-linear function which gives the crack length as a function of δ/P. Crack lengths can then be determined using graphs, tables or computed solutions of the appropriate a vs δ/P function.

In the case of the 1T-CT specimens, the calibration tests were performed at the test temperatures (93°C, 288°C) and the resultant expressions can be used without a temperature correction factor to account for changes in the LVDT calibration or in the elastic modulus of the test material. In the case of the 2T-WOL specimens, the basic calibration curve was developed at room temperature. A temperature correction factor was computed by noting the shift in /P produced in six specimens of varying crack length when they were raised to temperature (288°C) at the start of their test. After the temperature difference in LVDT calibration coefficient is accounted for, the remaining shift should be a factor of the ratio of the elastic moduli of the material at room temperature (25°C) and at operating temperatures (288°C).

$$\left(\frac{\delta}{P}\right)_{25} = \left(\frac{\delta}{P}\right)_{288} \left(\frac{E_{288}}{E_{25}}\right)$$

where E is Young's Modulus for the material. The ratio computed is 0.933. The accuracy of this ratio has been substantiated by comparing the initial and available beachmarked crack length readings on all subsequent tests with the corresponding crack lengths accurately measured on the fatigue fracture surfaces using traveling microscopes and recomputed using a seven-point averaging technique.

While the accounting for the temperature dependence of the LVDT's and the elastic modulus eliminates the major sources of error, other variables could perturb the accurate measurement of crack growth. Among these are thermal transients in the autoclave environment, unexpected aging of the LVDT or conditioner, seal friction losses, mechanical losses in the LVDT mounting hardware and undesired restraint in pin rotation in the clevis grips or in the specimens. However, in the face of all this, the fact remains that nearly all the compliance inferred crack lengths match up within about 0.008 W of the post test, optically measured crack lengths, implying that these errors do not significantly affect the final results.

Data Acquisition

In the three years of testing during which these data were developed, several improvements in the data acquisition procedure were made, culminating recently in the installation of a computer controlled data acquisition system which handles the acquisition responsibilities for all six test stands with a minimum of operator interaction. The earliest methods involved holding the loads at roughly 20% and 80% of the maximum, reading the LVDT outputs on a digital voltmeter and computing the displacement/load slope. The next stage of improvement resulted from the use of digital oscilloscopes to record load and LVDT output for five consecutive load cycles, digitizing about ten matched pairs from each of the load vs time and LVDT vs time slopes, computing displacement/load slopes, and using the average of these five to compute crack lengths. The computerized method is similar to the above, but uses one hundred pairs of automatically acquired points to compute the slope. More complete details are given in Ref [2].

Data Reduction

The methods used to process the crack length vs cyclic count data are very similar to the methods of ASTM Standard E647-78, "Methods for Fatigue Crack Growth Rate Testing for Rates 10^{-8} m/cycle." The a vs N values are computer processed using an incremental polynomial method which differs from the ASTM (7 point) method only in that a larger number of data points (up to 19) may be included in each increment. Use of this feature is necessary for those data sets acquired by the computerized data acquisition system. These data sets contain a larger number of points, spaced more closely, and with slightly more variability, than called for by the ASTM practice. In this report all data from specimens of the "F" material code were processed using the 7-point ASTM method, while the "R"-code forging data was processed using a larger number of points per increment.

The current ASTM practice indicates that one criterion for validity of crack growth rate data is that the unbroken ligament of the specimen (W-a) must satisfy the inequality

$$W - a \geq 2.5 \left(\frac{\Delta K}{\sigma_{ys}} \right)^2$$

at all times during the test, where

W = specimen width

a = crack length .

σ_{ys} = 0.2% offset yield strength of the material at test temperature

R = load ratio

ΔK = applied stress intensity range, computed using the formula in E647-78.

Prior to the introduction of this requirement, some data were recorded that would now be deemed invalid. Some of these data exhibited no change in trend as the crack extended beyond the lengths for which Eq. 2 was validated. An experiment was conducted to determine if these data could be qualified. This involved testing of two 2T-WOL specimens of A533-B material such that within an overlapping ΔK range, one specimen produced "valid" data while the other specimen produced invalid data. The details of this are given by Ref. [3], and the results indicate no significant differences in the data acquired from either specimen. Additional research by James [4] indicates the same conclusion.

Fractography and Metallography

The SEM specimens used to examine the fracture surfaces were machined from failed fatigue specimens to a size of approximately 20.0 mm x 9.0 mm x 3.0 mm. The specimens were ultrasonically cleaned in alcohol and acetone to remove oil deposits and loose scale. The fractographic examination was carried out using two different scanning electron microscopes: a Coates and Welter field emission microscope and a ISI Super II microscope. Both electron microscopes were operated at an acceleration voltage of 20 kV.

For metallographic examination, longitudinal sections were cut along the midplane of the specimens perpendicular to the fracture surfaces. For edge retention, some of the sections were electroplated with 0.25 mm (0.01-in.) thick layer of nickel prior to metallographic polishing. All the polished sections were etched for about 30 sec in 1% nital solution and examined optically and with a SEM to determine the relationships between the microstructure and the crack path. The optical micrographs were taken with a Bausch and Lomb Research II metallograph, the SEM micrographs were taken with the ISI Super II. The microstructure of one polished and etched Section (R1-1) was examined with an AMR 1000 SEM equipped with an EDAX Model 707B dispersive energy x-ray analyzer. The X-ray analyzer was used for the possible identification of second phase particles such as inclusions and precipitates.

RESULTS OF CRACK GROWTH RATE STUDIES

The fatigue crack growth rate data acquired under the preliminary matrix test plan is shown in Figs. 4-6. The figures are paired according to certain characteristics of the waveforms and in all three cases, the lower temperature (93°C) results are on the left and the higher temperature (288°C) results are on the right. There are three factors which strongly influence the crack growth rates in A508-2 in the reactor grade water environment; these are the prime variables of the preliminary matrix scheme: rise time, hold time and temperature. An interrelationship among the three determines the particular crack growth rate; it is impossible to isolate one variable without fixing the other two.

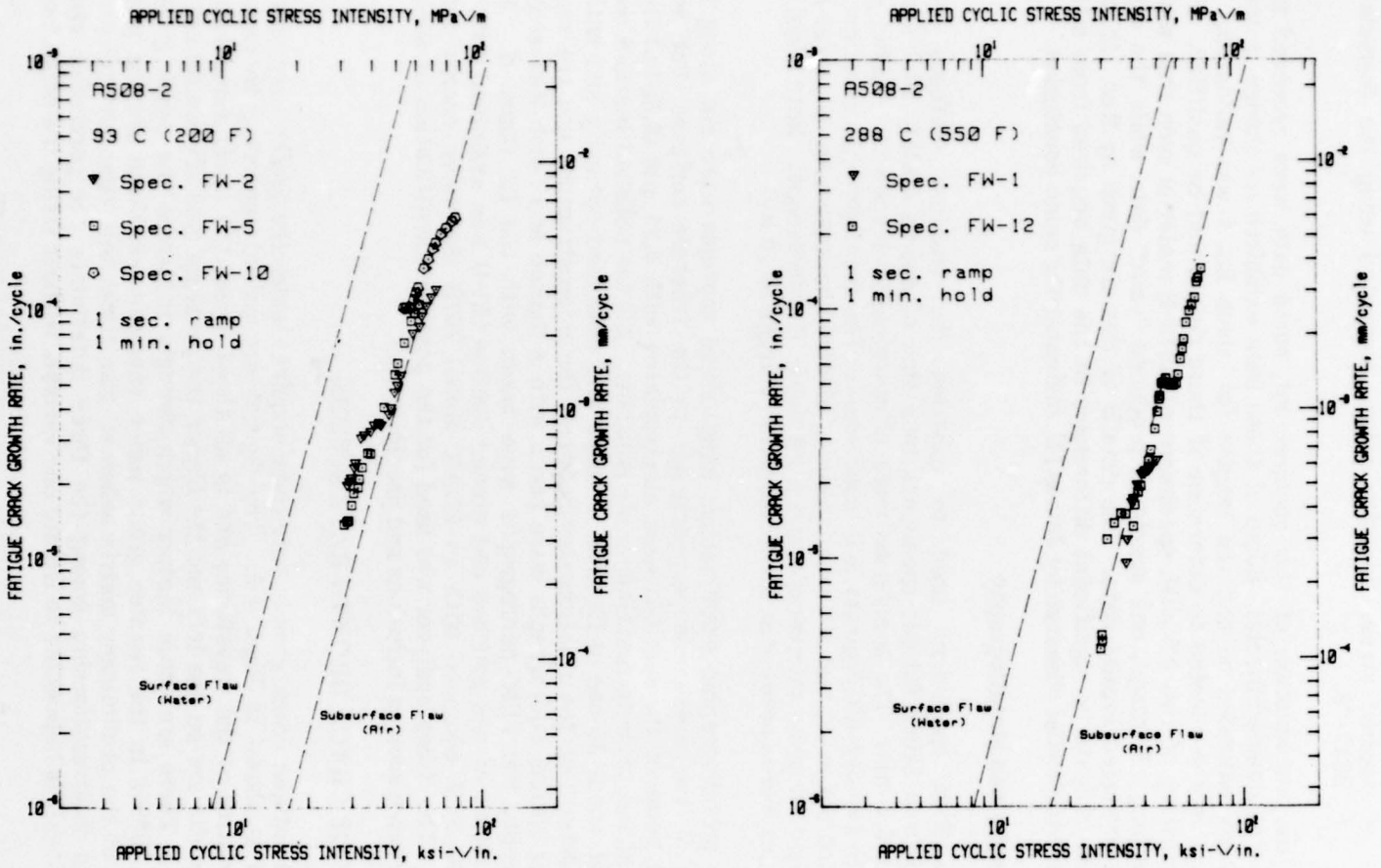

Fig. 4a, b. Fatigue crack growth rate data vs applied cyclic stress intensity for all the tests with a very short (1 sec) rise time. In this and the two following figures, the lower temperature test results are on the left. Both these temperatures yield growth rates close to the ASME Sec XI air default line.

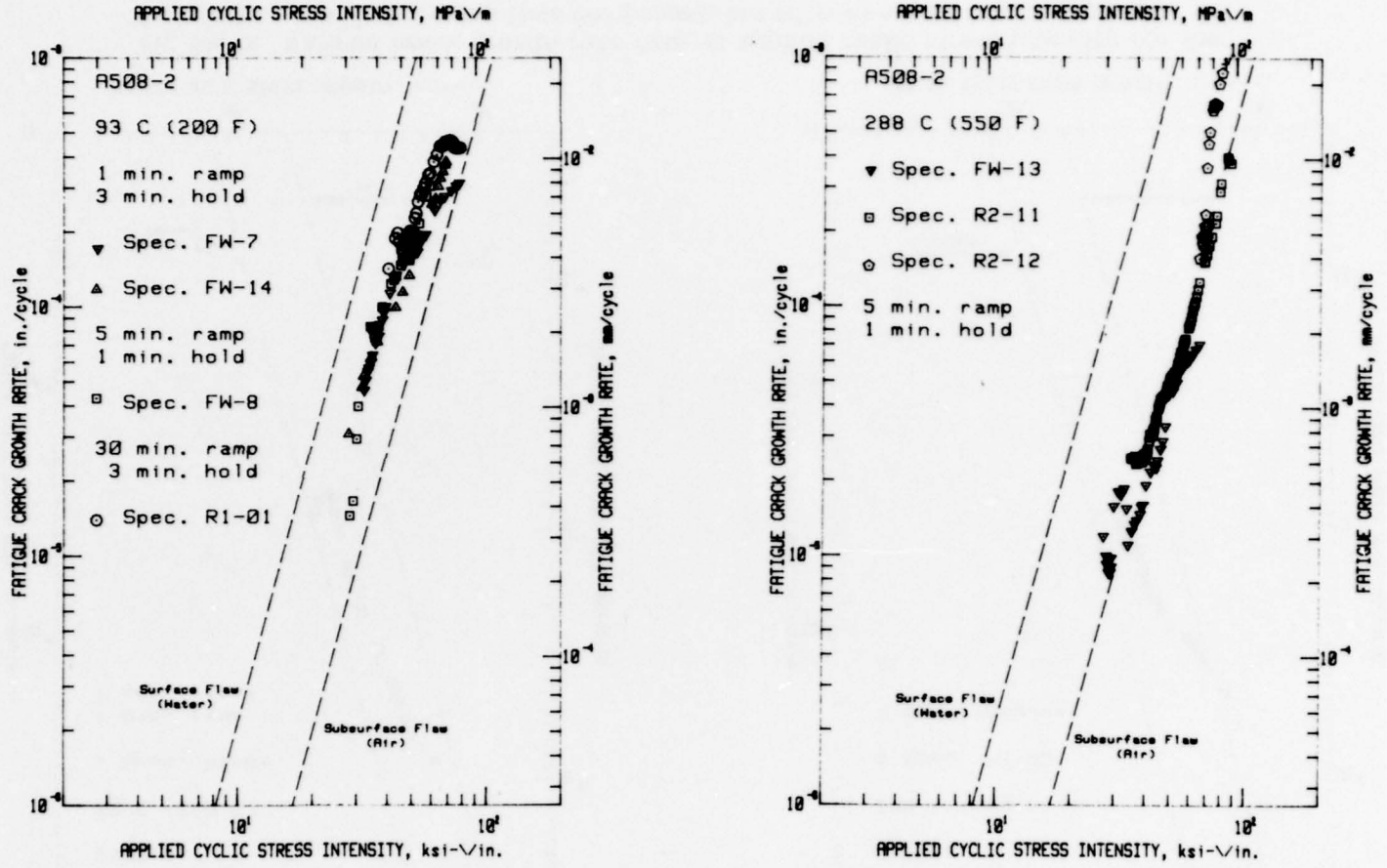

Fig. 5a, b. Fatigue crack growth rate data vs applied cyclic stress intensity for all the tests with both significant ramp times and hold times (1 min or greater for each). In the left hand data sets, the effect of the increased growth rates due to the lower temperature is clearly seen.

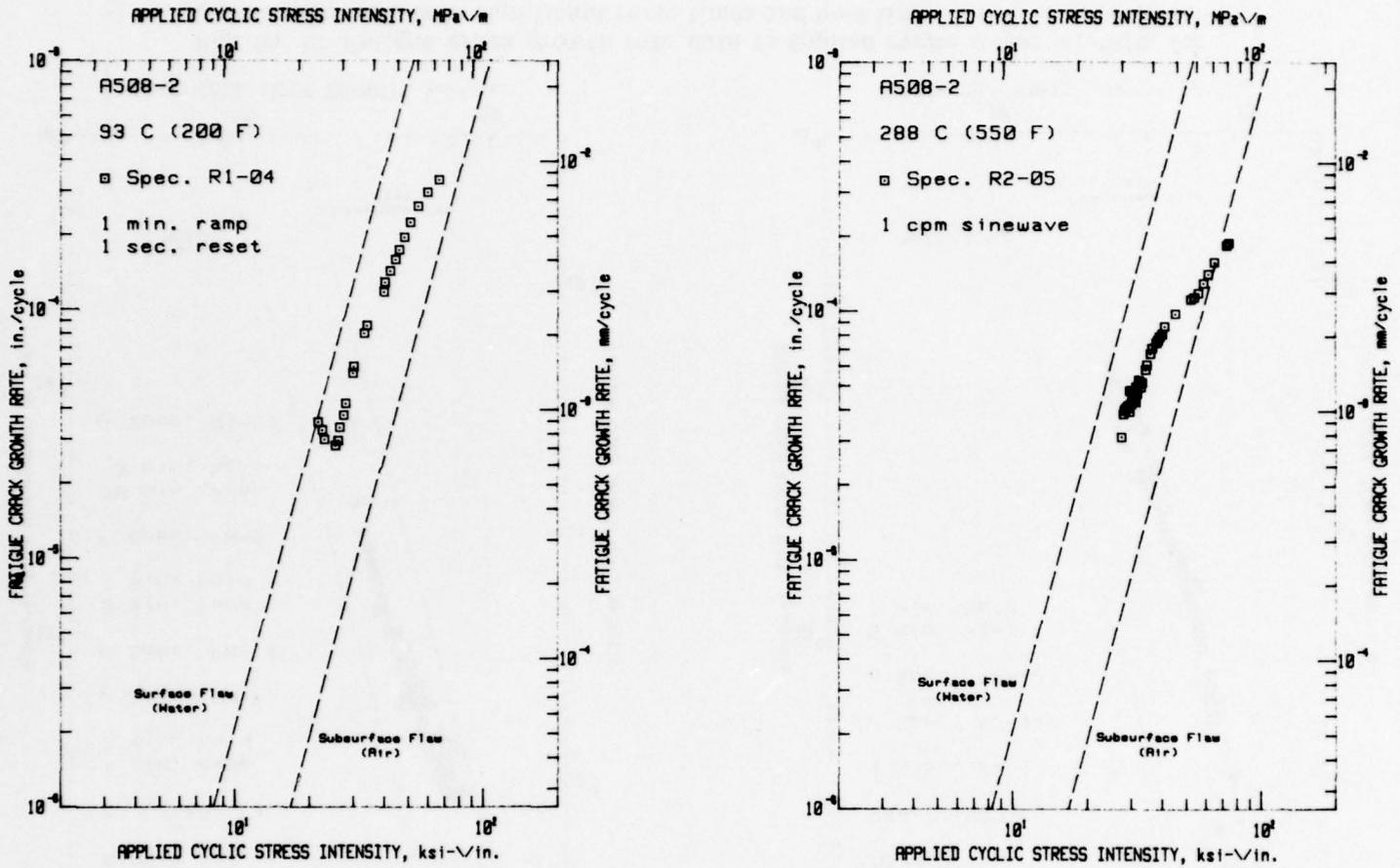

Fig 6a, b. Fatigue crack growth rate data vs applied cyclic stress intensity for the tests with a significant ramp time component, but without a hold time component. In these cases, temperature has little effect and growth rate data resides midway between the ASME Sec. XI air and water default lines.

An examination of all of the data sets produced under the guidelines of the preliminary matrix, together with other tests run under similar environmental conditions but utilizing non-matrix waveforms, indicates that data sets fall into one of two rather clearly defined categories. One band of data lies close to, or essentially on, the ASME Section XI Code air environment default line. This class of data, exhibiting the lower of the two crack growth rates, will be called "low." The other band of data, which resides a factor of three to five above the first, will be termed "high." This latter band of data resides approximately midway between the Section XI air and water environment default lines.

The two bands of data are the result of certain combinations of waveform and temperature variables and residence in one of the two is determined by the following rules:

(a) A ramp time in excess of one second is needed to obtain the higher crack growth rate. Several tests with a one second rise time (FW-1, -2, -5, -10, -12) all resulted in data sets falling in the low rate category. Other tests (FW-7, -14, -8, R1-01, -04, R02-05) with ramp times ranging from thirty seconds to thirty minutes produced data belonging in the high category, however, the other variables affect the exact nature of the results.

(b) The application of a hold time, together with a high temperature, serves to depress a normally high crack growth rate test (i.e., one with a long ramp time) and force it into the low category. It is clear from examination of the available data, that both the above variables (sufficient hold time, high temperature) must be present in the order to bring about the repression of an otherwise high growth rate test (FW-13, R2-11, -12). Tests in which one variable was absent such as R2-05, high temperature only,(no hold time) or FW-7, -14, -8, R1-01, hold time only (low temperature) resulted in high crack growth rates.

Permutation of the three variables and the results produced by them in conjunction with each other, leads to construction of two tables, 2a and 2b.

While these data sets are rather self consistent within a grouping, individual plots exhibit small irregularities in behavior. Small plateaus, reversals and accelerations which result in deviations from power law behavior are features of many of the data sets. There is no clear-cut explanation for these features, but they are most likely related to interruptions in the test program, or to unavoidable changes in the environment, temperature, water pressure or other test variable. These irregularities are the subject of continued study and documentation.

A single test, at 288^{o}C, with a triangular waveform (1 min rise, 1 min reset) produced results which are incongruent with the balance of these tests. It would be expected (Table 2b) that a "high" crack growth rate would be found in this zero hold time test. However, as shown in Fig. 7, a decidedly "low" growth rate is indicated. There were no significant experimental difficulties associated with this test which would call the results into question. Additional tests of similar waveforms are underway and speculation of a possible mechanism for this apparent exception is contained in a later section.

Table 2

Summary of the Dependence of Fatigue Crack Growth Rates on Temperature, Rise Time and Hold Time

Table 2a Tests with Long Hold Times

	short rise time	long rise times
low temp	low	high
high temp	low	low

Table 2b Tests with No Hold Time

	short rise time	long rise time
low temp	not attempted	high
high temp	not attempted	high

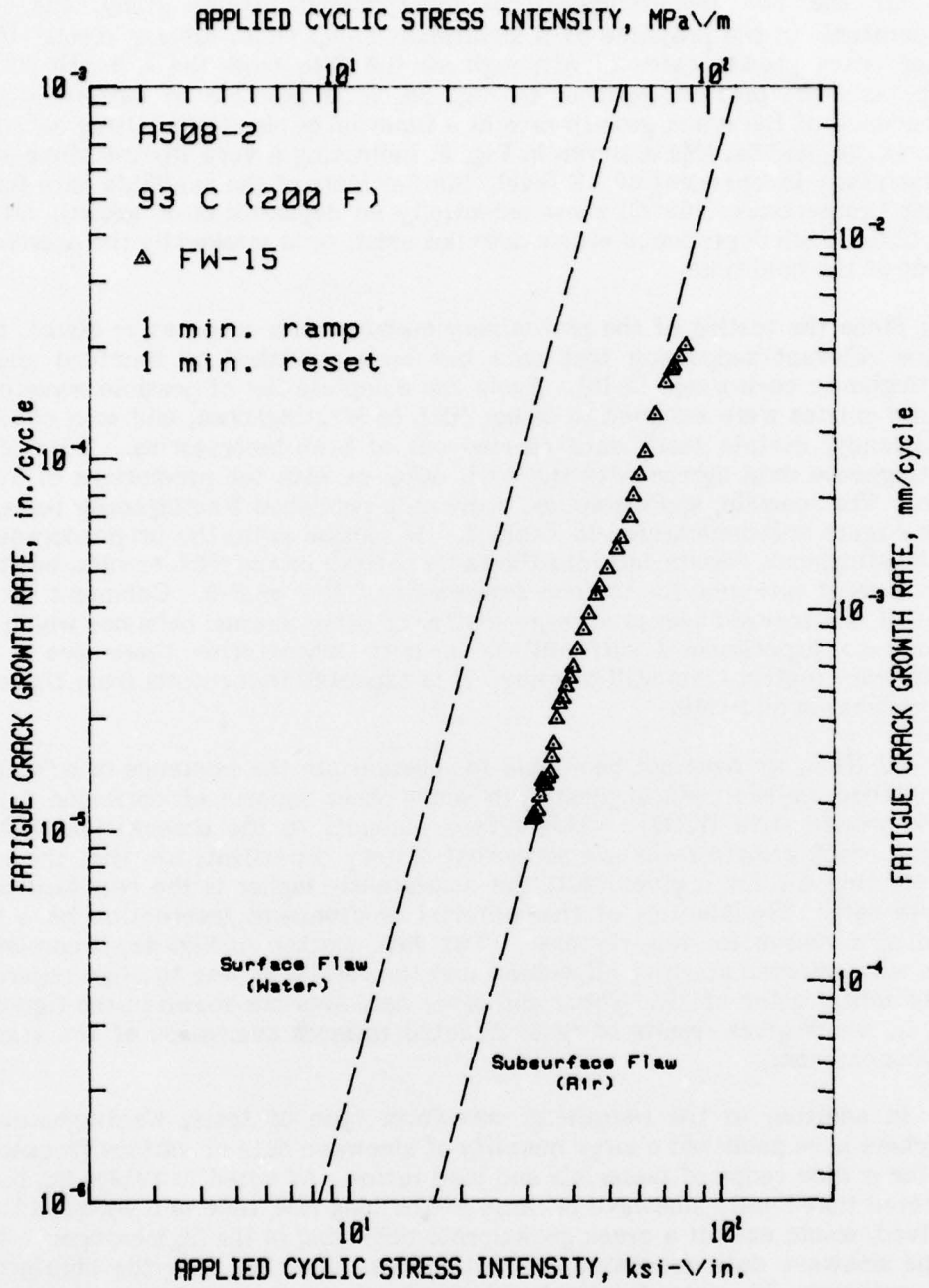

Fig. 7 Fatigue crack growth rate data vs applied cyclic stress intensity for specimen FW-15. This test, at 288°C, had a one minute ramp, one minute reset load waveform, and would be expected, on the basis of Table 2b, to exhibit growth rates in the high category. A possible explanation for the alternative behavior is advanced in the section on mechanisms.

Of the two test temperatures incorporated in this study, the lower temperature, in the presence of a significant ramp time, clearly results in the higher crack growth rates . Although all the data from the 1, 5 and 30 min. ramp tests are plotted together in Fig. 5a, it is possible to discern a slight dependence of the crack growth rate as a function of rise time. Using data from Figs. 4a, 5a, and 6a, this is shown in Fig. 8, indicating a very shallow slope which is essentially independent of ΔK level. Similar plots of the available data for the higher temperature (288^{o}C) show essentially no dependence of growth rate on rise time. Such dependence either does not exist, or is masked by the passivating effect of the hold time.

Since the testing of the preliminary matrix was a cooperative effort, much of the relevant supporting test data has been published by Bamford and his Westinghouse co-workers [5-10]. From the complete list of possible waveforms, certain entries were assigned to either NRL or Westinghouse, and as a check on consistency, certain tests were carried out at both laboratories. Most of the Westinghouse data agrees with the NRL data, or with the predictions of Tables 2a, b). The specific, applicable and previously published Westinghouse tests, and their results are summarized in Table 3. As can be seen, the preponderance of the Westinghouse results fall into the same pattern as the NRL results, but there is no current rationale for the non-agreement of R-8 or F-9. Comment on F-10 and F-11 is reserved because of large scatter or other unusual behavior which may be due to experimental difficulties. In both laboratories there are a few preliminary matrix tests still ongoing. It is expected that results from these will be available in mid-1979.

At NRL, we have not been able to substantiate the existence of a "starting ΔK" effect, as has been suggested in some other reports of corrosion fatigue crack growth data [7, 12]. This effect amounts to the observation that the fatigue crack growth rates are somewhat history dependent; i.e. that the lower the starting ΔK for a given test, the consistently higher is the resultant crack growth rate. The kinetics of the material environment interaction have been cited as a reason for this response. The data plotted in Fig. 4a, b consists of tests with assorted starting ΔK values, and the results appear to align regardless of the initial value of ΔK. These and other data sets are shown in the figures of Ref. 11, which gives results of tests directed towards evaluation of the starting ΔK phenomenon.

In addition to the ramp/hold waveform type of tests, Westinghouse researchers have published a large quantity of sinewave data of various frequencies and for a wide range of materials and load ratios. As noted in Tables 2a, b, it is expected that 17mHz sinewave because of the long rise time and zero hold time involved, would exhibit a crack growth rate belonging in the high category. Most of the sinewave data generated at Westinghouse does fall into the high growth rate category. In other Westinghouse work, there are also some interesting effects of frequency and specimen size which should be noted. For high sinewave frequencies (>1 Hz) it would be expected that the environment would not have time to aggressively contribute to the crack growth rate and the rate might trend into the low category. Similarly, for very low frequencies (>2 mHz

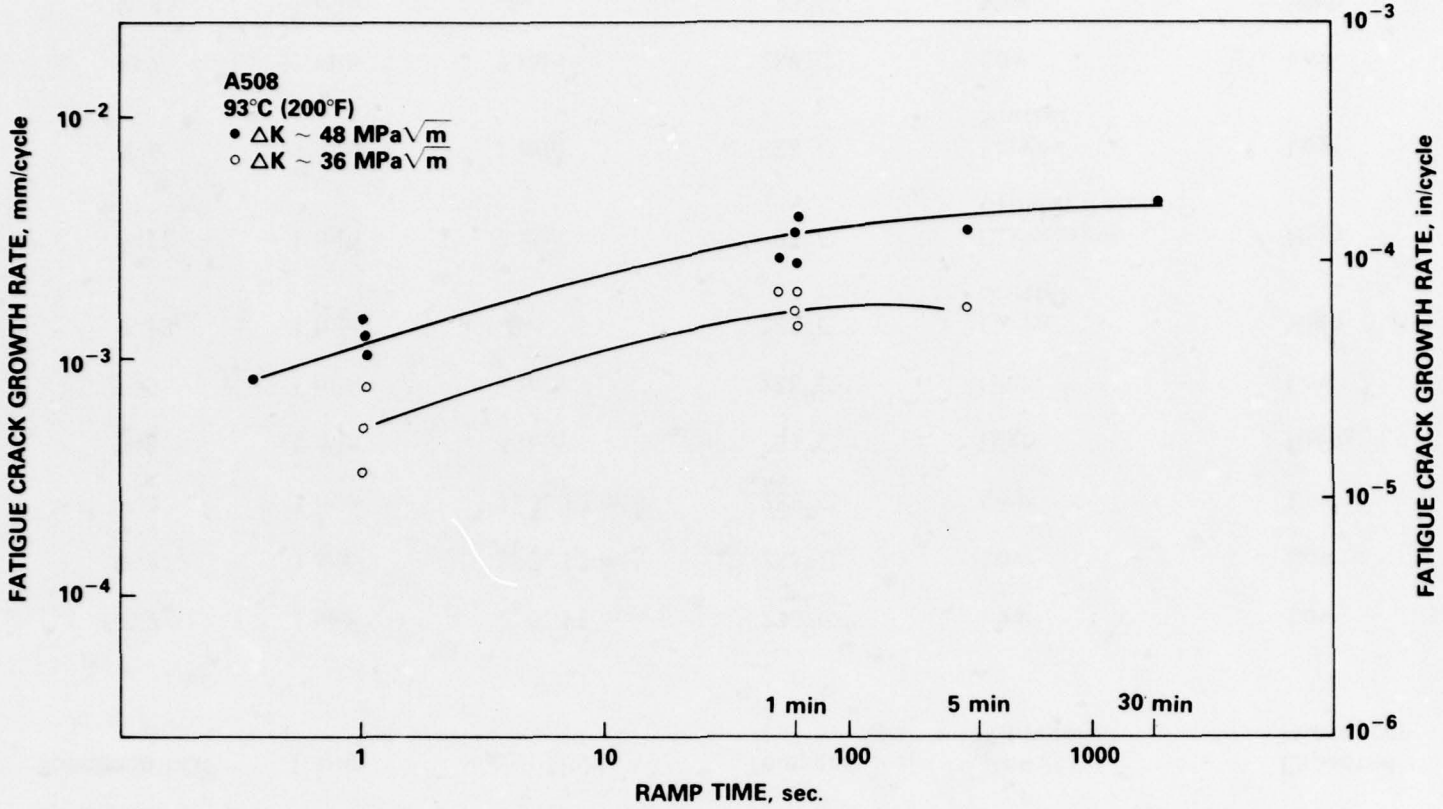

Fig. 8 Fatigue crack growth rate, for two values of applied cyclic stress intensity vs ramp time. These data sets are for the low temperature (93°C) condition and show a slight dependence of the growth rates on increasing ramp time. The high temperature growth rates exhibit very little dependence on the ramp time and are not shown in this report.

Table 3

Summary of Westinghouse Results

Specimen I.D.	Ramp	Hold	Temperature	Resultant Category	Expected Category
F-2	1 sec	1, 3, 12 min	288°C	Low	Low
F-3	1 sec	1, 3, 12 min	288°C	Low	Low
F-4	1 min	1, 3, 12 min	288°C	Low	Low
F-8	1 min	3 min	93°C	High	High
F-9	1 min	1 min	288°C	High	Low
F-10	1 min	-0-	288°C	Large Scatter	High
F-11	1 min	3 mm	93°C	Decreasing Growth Rate	High
R-6	5 min	1 min	288°C	Large Scatter	Low
R-7	1 min	3 min	288°C	Low	Low
R-8	1 min	-0-	93°C	Low	High

or less) the same passivation mechanism which causes low growth rates in hold time/high temperature tests might also be able to assert itself against such a slowly varying waveform. Consideration of several Westinghouse tests, utilizing a range of frequencies of sine waveforms tend to show that 17mHz sine waveforms produce the highest crack growth rates while faster (≥ 100 mHz) and slower (1.7, 8.5 mHz) tend to produce slightly lower crack growth rates [5,6]. Both the NRL and Westinghouse sinewave tests exhibit a "bend-over" characteristic for the higher (>50 MPa$\sqrt{m}$) ΔK levels. This behavior is, however, <u>not</u> a characteristic of the ramp-and-hold type of waveform. While the data sets are clearly positioned in the high growth rate category for lower ΔK levels, the growth rates for sinusoidal waveform diverge from a power law type of behavior, and trend to lower growth rates, often crossing to the right-hand side of the Section XI air default line. At the present time, such behavior has been clearly noted for sinewave loadings, and a possible mechanism for this is advanced in a later section of this report.

Support for some of these observations and conclusions can also be found in the published results of several other investigators. Kondo et al. [13] published the results of corrosion fatigue tests on A533-B at 260°C in pure water of higher oxygen content (~1 μmho/cm and ~70 ppb dissolved oxygen) which is more characteristic of a boiling water reactor (BWR) system. These tests utilized either square or sinewave load patterns and the main conclusion is that growth rate increased steadily as the test frequency decreased from 1.6 Hz (100 cpm) to 0.005 Hz (0.3 cpm). As noted above, this is reasonably consistent with the Westinghouse results, and the lowest frequency (0.005 Hz) would be about the point at which the trend might reverse --even lower frequencies leading again to lower crack growth rates. It is also possible that the different environment, specifically the higher oxygen content of the BWR-type systems, may result in crack growth rates which monotanically increase with ramp time.

In a second reference Suzuki et al [14] Japanese researchers measured crack growth rates for A533B in a heat affected zone at three temperatures, 50, 85 and 260°C. Although only a few data points were published, these suggest that for 0.016 Hz (1 cpm) sinewave loadings, a maximum in growth rate is attained at approximately 200°C, while 93 and 288°C (the two temperatures of this study) would both produce lower (and about equal) crack growth rates. At the lower temperature regime, this conclusion is substantiated by the published results of Pacific Northwest Laboratories [15]. These data, developed for the much higher frequency of 2 Hz, showed that growth rates at 93°C were higher than those at 24°C. Since neither the Kondo, the PNL nor the NRL data are conclusive on this issue of temperature dependence, this should be singled out as an area for future research.

METALLOGRAPHY

The basic aims of the metallographic examinations were (1) to investigate the relationship between the microstructure and the crack path, and (2) to identify the various microstructural components, such as carbide particles, inclusions and oxidation products and the possible influence of these components on fatigue crack propagation behavior.

In Fig. 9 are optical micrographs of transverse sections of specimens tested at the lower temperature. The top two micrographs show that specimens tested with short rise time (FW-5 and FW-2), (1 sec) had shallow and mostly transgranular crack branching. The bottom micrographs typify the microstructure and the crack path of specimens tested with long rise time (FW-7 and FW-8) (1 min and 5 min respectively). The crack path and crack branching for the two latter specimens were mostly transgranular but some intergranular paths appeared to be present also. The secondary cracks were larger and deeper than in the previous two specimens. Photomicrographs shown in Fig. 10 refer to specimen FW-13 (tested in the autoclave) (top micrographs) and specimen Q71-3* tested in air (bottom micrographs) both at 288°C. As shown by the micrographs, the crack path and the branching are transgranular, and an oxide layer appears to be present in some of the secondary cracks (Fig. 10b and c). This oxide layer may protect the crack and thereby reduce the crack growth rate.

Photomicrographs shown in Fig. 11 refer to the crack profiles of specimens R1-1 and R1-2, the former tested at 93°C and the latter at 288°C. The loading waveform for specimen R1-1 consisted of a 30 min rise and 3 min hold time and that for R1-2** was comprised of 1 min rise and 60 min hold time. As shown by the photomicrographs in Fig. 11, the basic difference in the crack profile in the two tests is the extent and the type of secondary cracking. The microcracks in R1-1 are rather large and deep. On the other hand, the average number of microcracks per unit length in R1-2 is much larger than in R1-1, while their average size is smaller. The microcracks in R1-2 are covered by an oxide layer while no oxide layer was present in the microcracks of R1-1.

The transverse sections of the same two specimens (R1-1 and R1-2) were also examined with the SEM; the significant observations of this analysis are summarized by the micrographs presented in Fig. 12. These SEM micrographs refer to the crack tip region of the two specimens.

The lower magnification micrograph on the top (Fig. 12) representing the crack tip of water pot test shows that the crack had branched at this point. The extensive branching at the tip of the crack would partially explain the pronounced bend in the fatigue data for this test in the high ΔK end (Fig. 5a), where it is believed that the specimen was about to yield. Micrograph 6 is a higher

---

*Specimen Q71-3 was not a part of this particular study, however, it was also A508 material, of the same essential chemistry as the heats above. For all practical purposes, it is expected to have the same fatigue properties. See Ref 16 for fatigue results of Q71-3. The waveform for specimen Q71-3 consisted of 1 sec ramp, 22 sec hold and 1 sec reset.

**Faulty LVDT behavior during test R1-2 prohibited acquisition of reliable crack growth rate data. The test was allowed to continue for the express purpose of obtaining micrographic and fractographic information. The overall crack extension in R1-2 was about 4 mm. The overall growth and cyclic count indicates a growth rate clearly belonging in the "low" category.

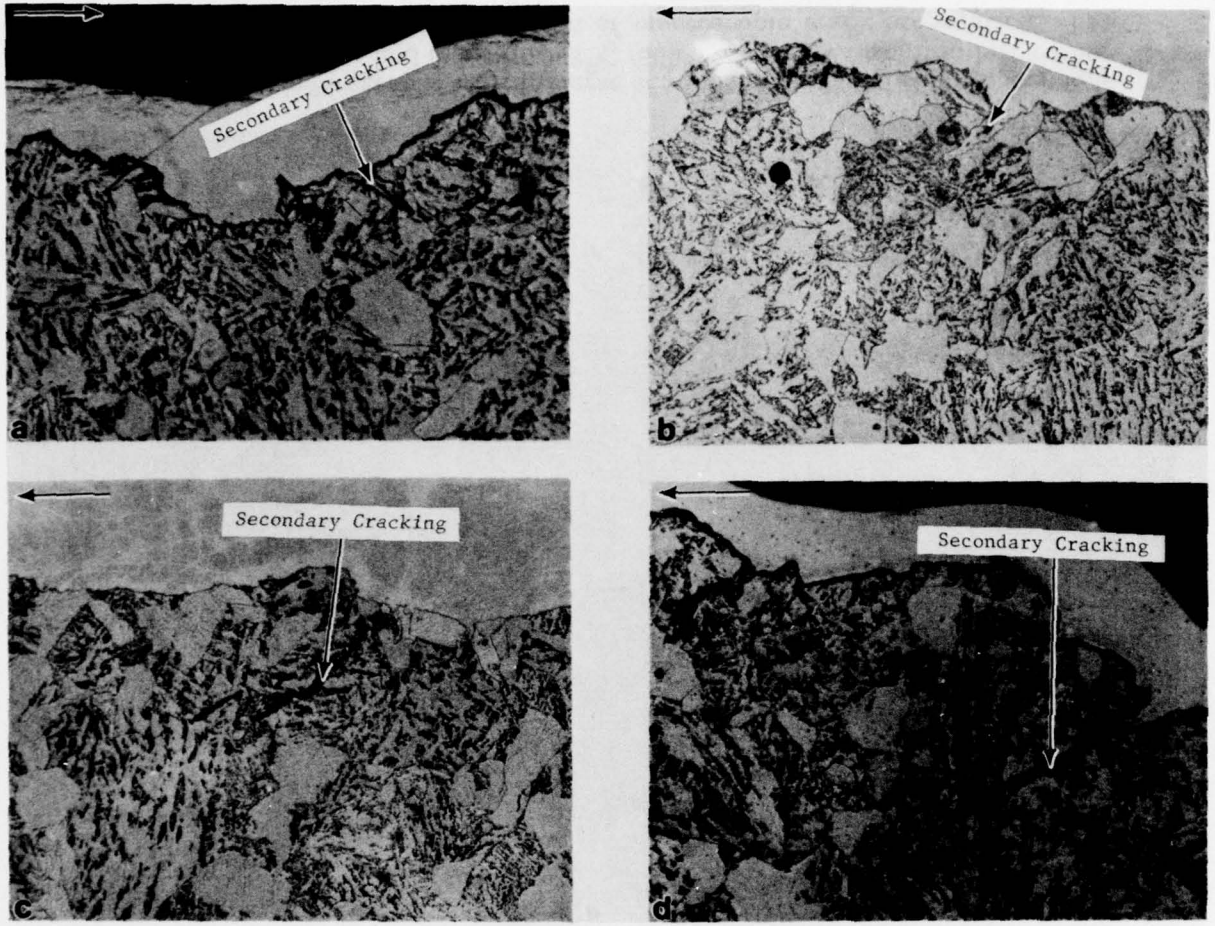

Fig. 9 Optical micrographs of transverse sections of A508-2 fatigue specimens tested in water pot (93°C, 200°F) with different loading waveforms. The arrow on top left corner of each micrograph indicates direction of macroscopic crack propagation. (a) specimen FW-5, (b) specimen FW-2, (c) specimen FW-7, and (d) specimen FW-8. The top micrographs show mostly shallow transgranular branching; the bottom micrographs show deeper transgranular and sometimes intergranular branching.

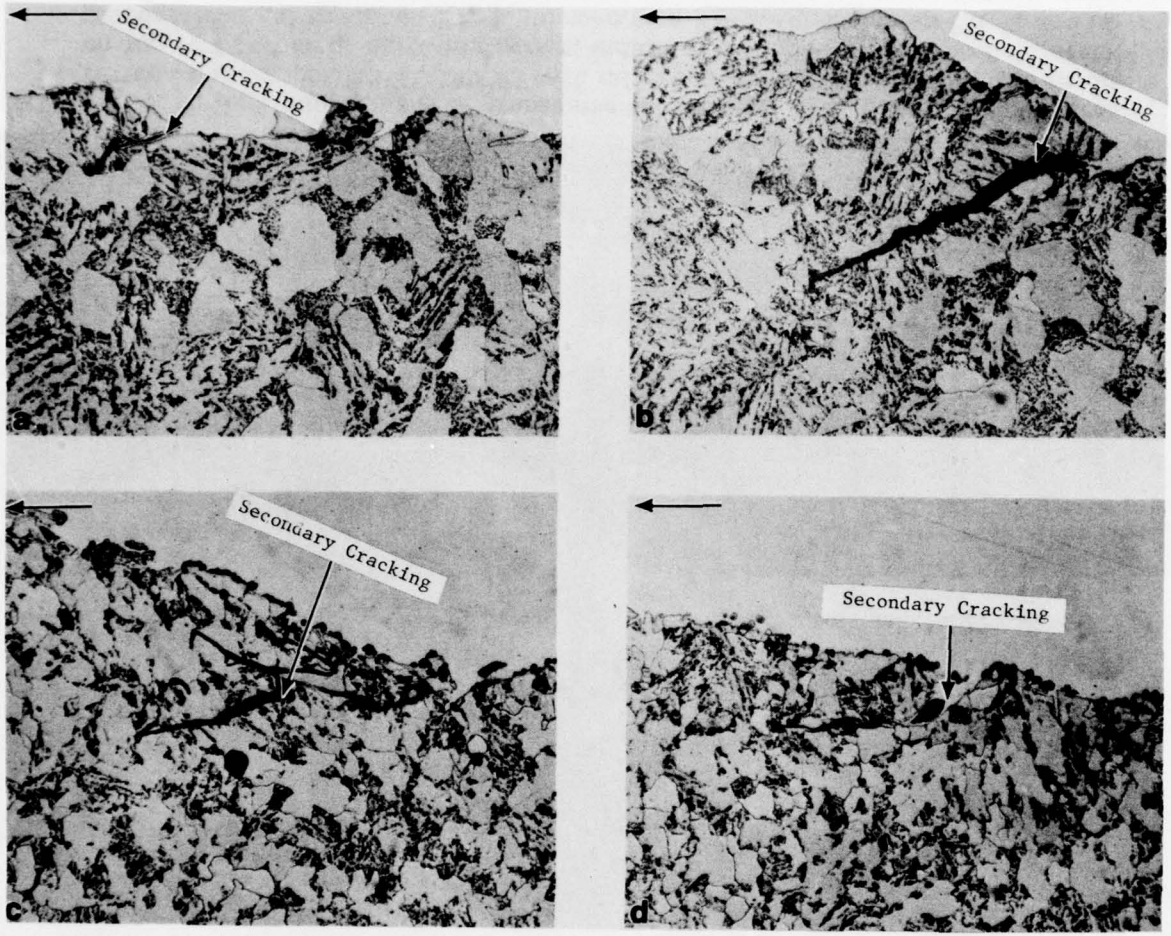

Fig. 10. Optical micrographs of transverse sections of A508-2 fatigue specimens tested in the autoclave and in air at 288°C (550°F). The arrow on top left corner of each micrograph indicates direction of macroscopic crack propagation. Top micrographs: specimen FW-13, bottom micrographs: specimen Q71-3. The branching in both specimens is transgranular.

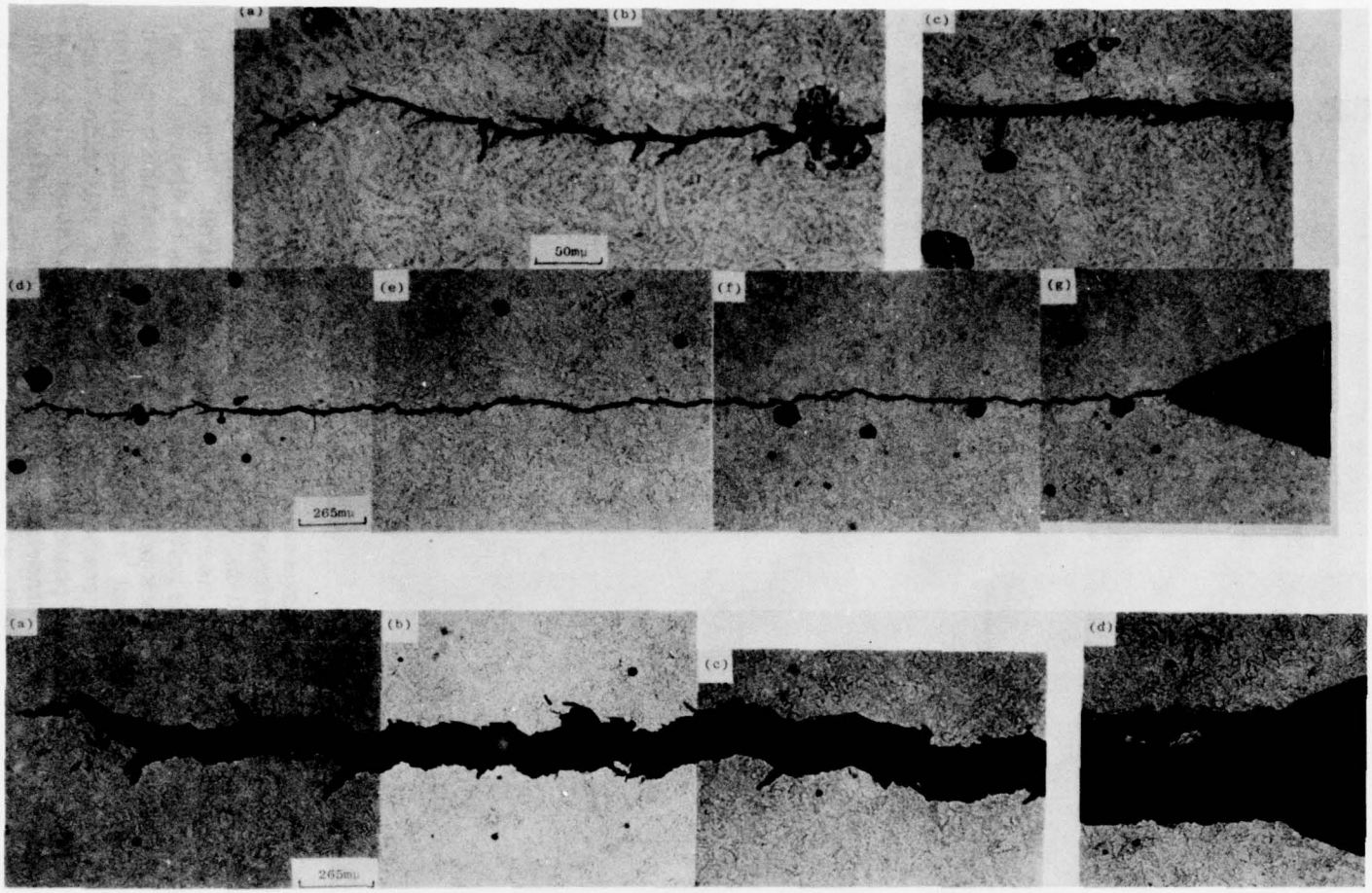

Fig. 11. Optical micrographs of transverse sections of A508-2 fatigue specimens tested in the autoclave (top micrographs, (a)-(g), R1-2) and in the water pot (bottom micrographs (a)-(d), R1-1). The specimen tested in the autoclave shows extensive branching with small microcracks. In the specimen tested in the water pot, the microcracks were larger but they were less than in the autoclave test. The average density of microcracks per unit length is roughly 5-6 times greater in R1-2 than in R1-1.

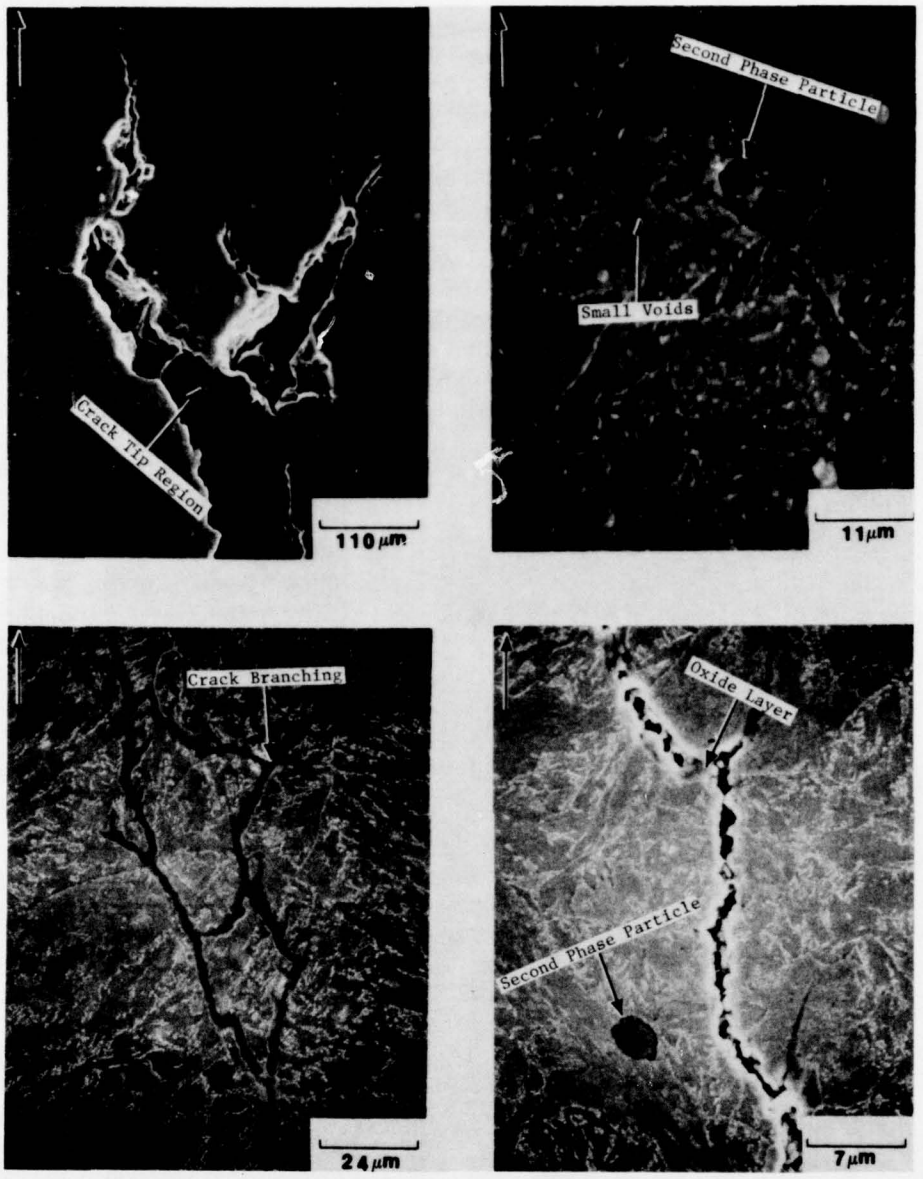

Fig. 12. SEM micrographs of transverse sections of A508-2 fatigue specimens; one tested in the water pot (top micrographs, R1-1) and the other tested in the autoclave (bottom micrographs, R1-2). The arrow on top left corner of each micrograph indicates direction of macroscopic crack propagation. Previous to SEM examination, the sections were polished and then etched in 1% nital solution. Micrograph (a) shows extensive crack branching; it is believed that the specimen has already yielded. The adjacent micrograph (b) is a higher magnification micrograph of a microcrack at the crack tip region. The tip of this microcrack shows a partially separated second phase particle surrounded by small voids. The bottom micrographs show crack branching and a second phase particle. The particle is not surrounded by small voids as in R1-1, while the crack path is covered by a protective oxide layer. No oxide layer was visible in specimen R1-1.

magnification micrograph of one of the branches of the crack tip of R1-1. With regard to this micrograph the following important points can be made. The secondary crack follows a path that leads to non-metallic particle believed to be an inclusion; the particle appears partially separated from the matrix material. The inclusion sites are considered to be locations to which hydrogen can most easily diffuse and be trapped. In addition, at the tip of the secondary crack, near the inclusion, there are some small voids that might represent hydrogen void develop ment ahead of the crack tip. These voids are seen in a band ranging up to 100 μm to each side of the fatigue crack with the greatest concentration within the thirty μm of material adjacent to the crack. Figure 12c and d are lower and higher magnification micrographs of R1-2 taken near the crack tip. Confirming the observations made through the optical micrographs (Figure 11c and d), these micrographs show that secondary cracks in this specimen are on the average smaller than in R1-1 and that all the secondary cracks appeared to be covered by a protective oxide layer. Fig. 12d shows a partially separated inclusion particle close to the crack path, but the particles are not surrounded by small voids as in the case of R1-1. Moreover, the particle is not located at the tip of a microcrack.

The micrographs in Fig. 13 represent the significant results of the crack tip examination of R1-1 by an AMR 1000 scanning electron microscope equipped with an energy dispersive X-ray analyzer, EDAX model 707B. The non-metallic particles shown in Fig. 13a, were analyzed with the energy dispersive unit. The results of this X-ray analysis, shown in Fig. 13 b-c, confirm that the non-metallic particle described above is an inclusion rich in both sulfur and manganese.

FRACTOGRAPHY

The fracture surfaces of many of the fatigue specimens included in the present study were examined by scanning electron microscopy (SEM). The fractographic analysis was undertaken with the aim of characterizing the failure processes and attempting correlations between the microstructure and the corres ponding fatigue properties, especially as they relate to the possibility of stress corrosion cracking (SCC) and/or corrosion fatigue* occurring in this low alloy steel tested at elevated temperatures in pressurized water.

Figure 14 shows typical SEM micrographs of fracture surfaces of two fatigue specimens tested in air at 288°C with two different loading waveforms. The top two micrographs refer to an air test with a trapezoidal loading composed of a one sec. ramp, 28 sec. hold, one sec. reset; the bottom micrographs refer to an air test with a one min. ramp/three min. hold waveform (R1-3). The micrographs show that the fractographic features are roughly the same for both specimens. The failure mode was transgranular with fatigue striation markings

---

*By stress corrosion cracking (SCC) is meant the subcritical crack growth that results in the presence of an aggressive environment under sustained load, while by corrosion fatigue is meant the subcritical crack growth resulting from the combined effects of cyclic stresses and aggressive environment.

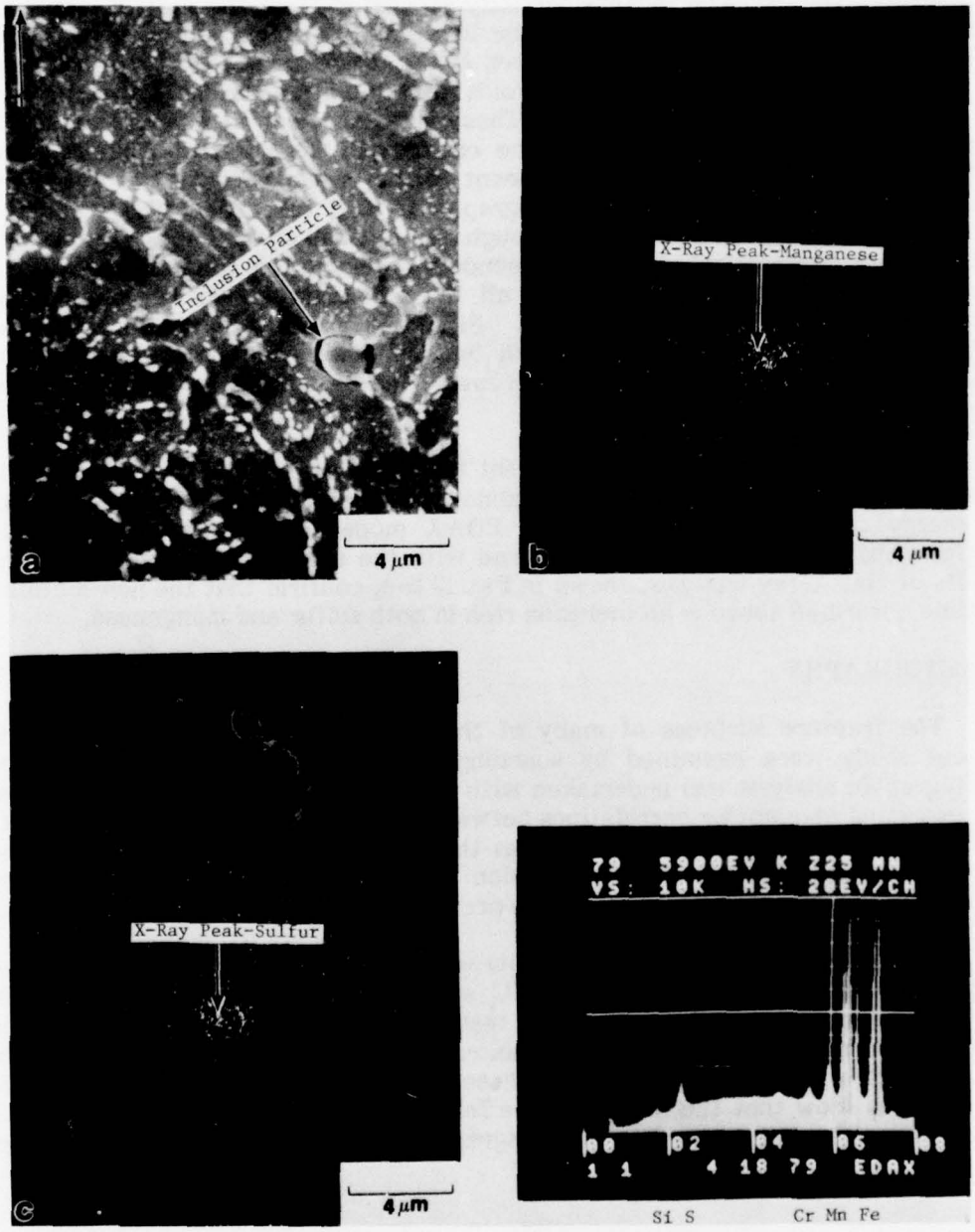

Fig. 13. SEM micrograph (a), X-ray scans (b and c) and X-ray energy spectrum of a second phase particle near the crack path of specimen R1-1. Arrow on top left corner and micrograph (a) shows direction of macroscopic crack propagation. The X-ray scans and corresponding X-ray energy spectrum show that the second phase particle is a manganese-sulfide inclusion.

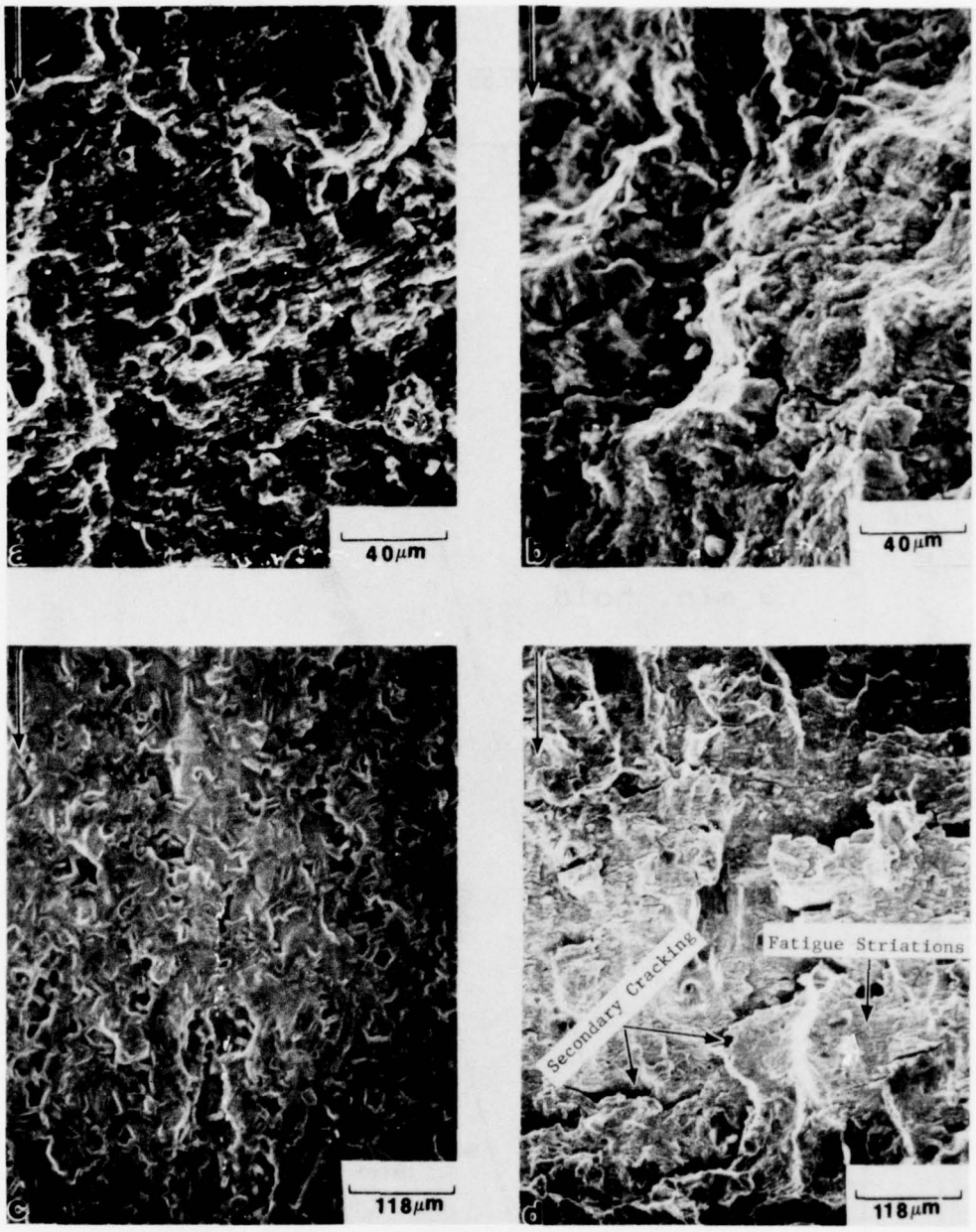

Fig. 14. Fracture surfaces of A508-2 fatigue specimens tested in air at 288° (550°C); top micrographs refer to specimen Q71-3, bottom micrographs refer to specimen R1-3. The SEM micrographs were taken at crack lengths that correspond to the following ΔK values: (a) 29.7 MPa$\sqrt{m}$ (27 ksi$\sqrt{in.}$), (b) 44 MPa$\sqrt{m}$ (40 ksi$\sqrt{in.}$), (c) 29.7 MPa$\sqrt{m}$ (27 ksi$\sqrt{in.}$), and (d) 63.8 MPa$\sqrt{m}$ (58 ksi$\sqrt{in.}$). Arrows show direction of macroscopic crack propagation. Micrographs show that the failure mode for both specimens was transgranular with fatigue striations and extensive secondary cracking clearly visible in the high ΔK region.

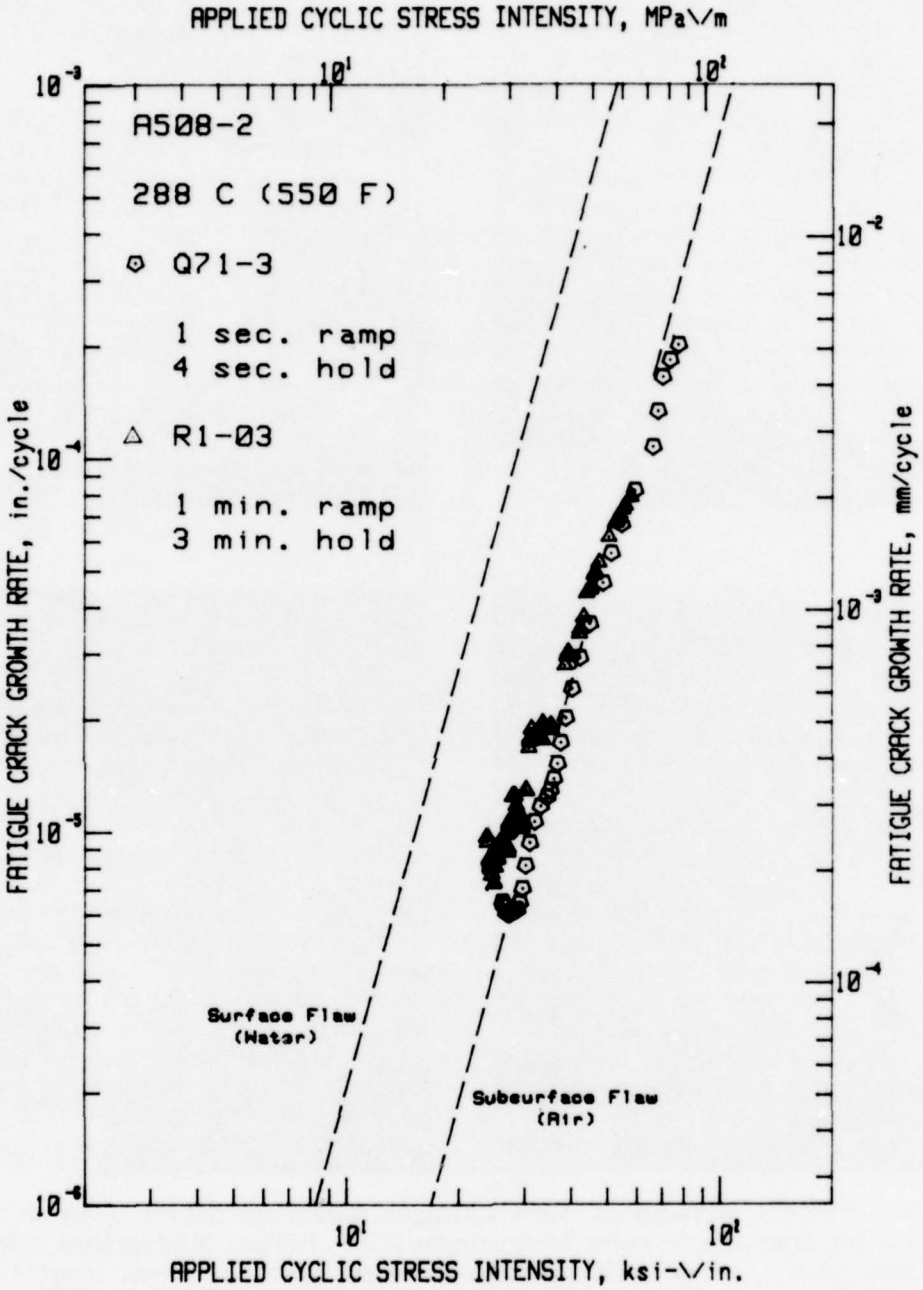

Fig. 15. Fatigue crack growth rate data vs applied cyclic stress intensity for two tests in an air environment at 288°C. Both of these tests, in an essentially dry (i.e. hydrogen free) environment exhibit data in the "low" growth rate category. As such, these observations are typical of crack growth behavior without hydrogen assistance.

that are clearly visible in the high ΔK region; extensive secondary cracking was also present for the entire ΔK range. Typical of ductile metals, the predominant failure process in these two specimens was plastic blunting accompanied by fatigue striation formation [17]. Therefore, the fractographic results of the air tests are consistent with the corresponding fatigue data. In fact, the crack growth rates for these air tests shown in Fig. 15, fall close to ASME Section XI air line, with the partial exception of the R1-3 specimen for which the crack growth rate in the low ΔK regime was slightly above the air line. The higher rate of R1-3 in the low ΔK regime is believed to be due to the combined effects of some transient, start-up phenomenon, coupled with the fact that the data in this region were subject to several equipment malfunctions, which were corrected and avoided for the balance of the tests. The SEM micrographs shown in Fig. 16 typify the significant observations made on the fracture surfaces of three specimens tested in 93°C reactor grade water with a ramp time of 1 sec but different hold time periods. The failure mode of the three specimens was transgranular with fatigue striations clearly visible in the high ΔK range. The striations are both irregular and discontinuous, and it is believed that they are partly obscured by oxidation products present on the fracture surfaces. (A more complete discussion of striation observation and measurement is given in Ref 18). The degree of secondary cracking appears to be somewhat less in these specimens than in the specimens tested in air. However, the basic fractographic features characterizing these tests in the water pot are very similar to those seen in the air tests. This leads one to conclude that the material tested in the water pot for the above test conditions resulted in a baseline behavior both in the failure mode and in the corresponding crack growth rate.

Fig. 17 summarizes the significant SEM observations on the specimens tested in 93°C water environment with waveforms of hold times comparable to those above, but with the longer ramp times of 3 min (FW-8) and 1 min (FW-7), respectively. As shown in the micrographs, the two specimens displayed similar fractographic features; the predominant failure mode appears to be transgranular, but no fatigue striation markings were seen in either specimen, and some regions of the fracture surface showed a trend to intergranular failure. In addition, local cleavage-like facets were present on some areas of the fatigue fracture surface. Secondary cracking was present on both fracture surfaces, although the cracking was not as extensive as in the case of the air tests; moreover, the average size of the secondary cracks was larger. The local cleavage facets and the lack of fatigue striations, together with some intergranular failure, are fractographic features that are commonly associated with mechanisms of SCC and/or corrosion fatigue. The possible presence of such a corrosion component would account for the accelerated crack growth rate in the specimens tested at the lower temperature, with ramp times of 1 min or longer, compared to the crack growth rates of specimens tested at the same temperature, and comparable hold times, but with the much shorter ramp time of only 1 sec.

In Fig. 18, the fractographic features of an A508 specimen, R1-04, tested at 93°C, with a one min ramp/one sec reset waveform are compared to the features observed in the same material, at the same temperature, but tested with a thirty min ramp, three min hold waveform (R1-1). The fractographic

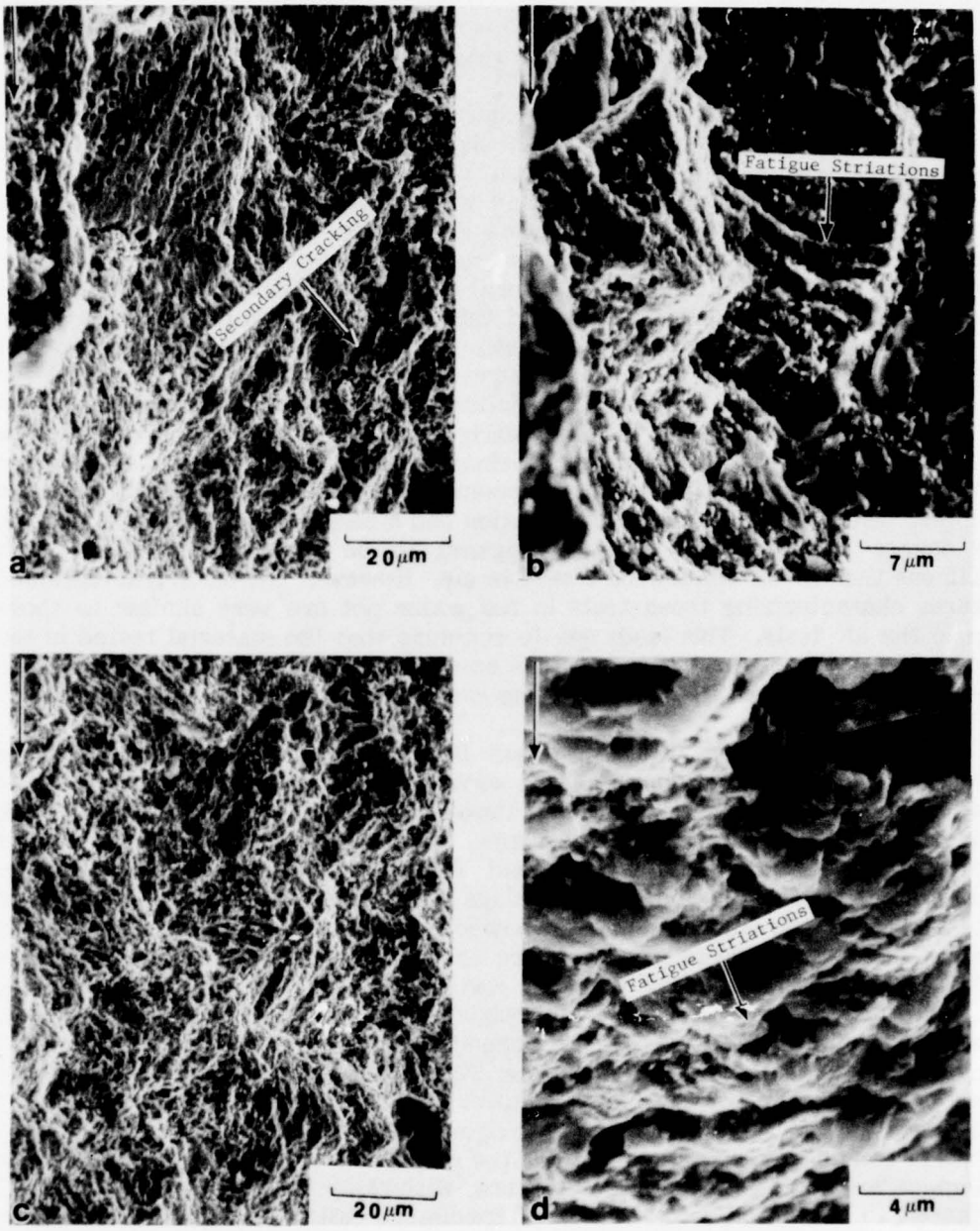

Fig. 16 Fracture surfaces of A508-2 fatigue specimens tested in the water pot (93°C,200°F), with different hold time periods but all with a ramp time of 1 sec. The SEM micrographs were taken at crack lengths that correspond to the following ΔK values: (a) 33 MPa$\sqrt{m}$ (30 ksi$\sqrt{in.}$), (b) 72.6 MPa$\sqrt{m}$ (66 ksi$\sqrt{in.}$), (c) 44 MPa$\sqrt{m}$ (40 ksi$\sqrt{in.}$), and (d) 88 MPa$\sqrt{m}$ (80 ksi$\sqrt{in.}$). Arrows show direction of macroscopic crack propagation. The failure mode for these specimens is transgranular with fatigue striations and secondary cracking, as in the air tests shown in previous figure.

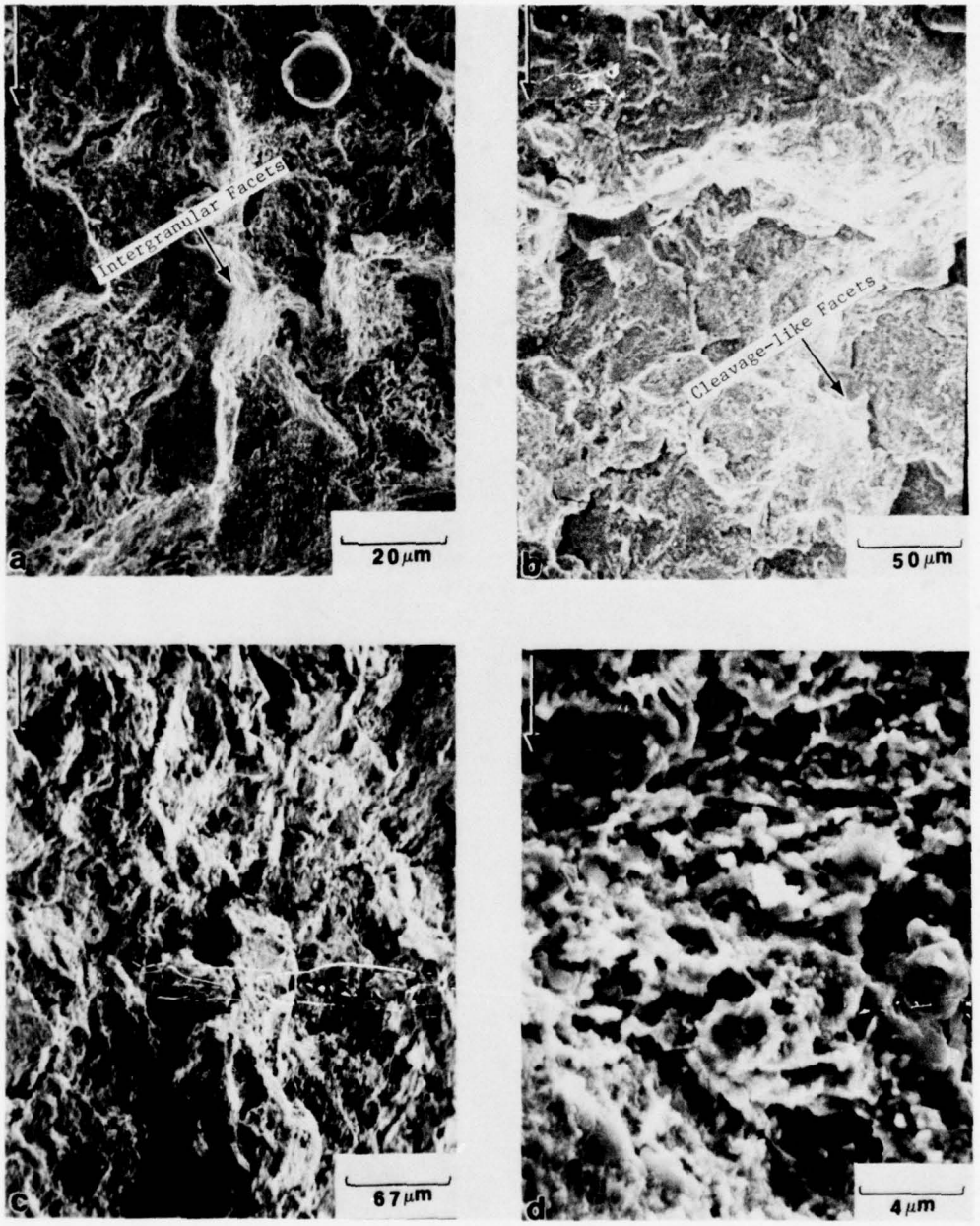

Fig. 17 Fracture surfaces of A508-8 fatigue specimens tested in the water pot (93°C, 200°F) with significant ramp and hold times (1 min or greater for each). (a) and (b) specimen FW-8, (c) and (d) specimen FW-7. The SEM micrographs were taken at crack lengths that correspond to the following values of ΔK: (a) 38.5 MPa$\sqrt{m}$ (35 ksi$\sqrt{in.}$), (b) 57.2 MPa$\sqrt{m}$ (52 ksi$\sqrt{in.}$), 33 MPa$\sqrt{m}$ (30 ksi$\sqrt{in.}$), and (d) 60.5 MPa$\sqrt{m}$ (55 ksi$\sqrt{in.}$). Arrows show direction of macroscopic crack propagation. As shown by the micrographs the predominant failure mode is *transgranular, but some regions of the fracture surfaces are characterized by* intergranular failure and by cleavage-like facets.

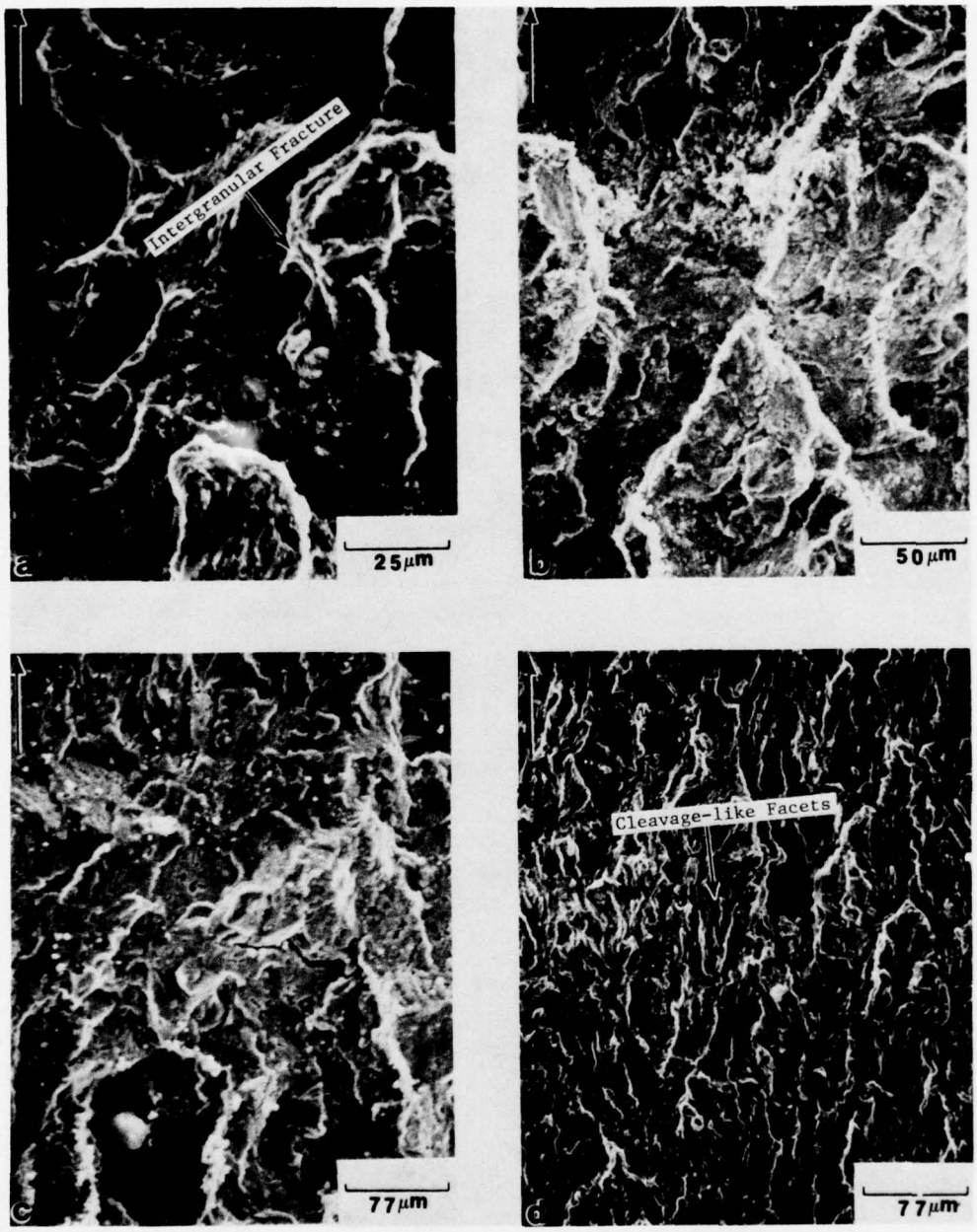

Fig. 18 Fracture surfaces of A508-2 fatigue specimens tested in the water pot (93°C, 200°F) with significant ramp time and no hold (R1-4, top micrographs) and with significant ramp and hold (R1-1, bottom micrographs). The SEM micrographs were taken at crack lengths that correspond to the following values of ΔK: (a) 25.3 MPa$\sqrt{m}$ (23 ksi$\sqrt{in.}$), (b) 66 MPa$\sqrt{m}$ (60 ksi$\sqrt{in.}$), (c) 40.7 MPa$\sqrt{m}$ (37 ksi$\sqrt{in.}$), and 66 MPa$\sqrt{m}$ (60 ksi$\sqrt{in.}$). Arrows show direction of macroscopic crack propagation. The fractographic features of these two specimens are similar to those observed in the water pot tests described in Fig. 3. Both sets of micrographs (Figs. 11 and 12) display fractographic features commonly associated with corrosion fatigue.

appearances of the two specimens are quite similar. That is, both fracture surfaces are characterized by quasi-cleavage facets, the absence of fatigue striations, some intergranular failure and sparse but large secondary cracks. These are nearly the same aspects observed in the other low temperature tests with waveforms that included hold times of 1 min or longer (FW-7 and FW-8, Fig. 17). Therefore, the features of R1-1 and R1-4 also indicate the possible presence of SCC and/or corrosion fatigue. The crack growth rates of both specimens were accelerated with respect to the ASME Section XI air line. (Figs. 5a and 6a). The results of R1-1 and R1-4 together with results of the other tests with trapezoidal loadings tend to indicate that at the 93°C temperature, the length of the hold time does not appear to be important, while the length of the rise time is the significant variable. This conclusion reinforces the practice of plotting Fig. 8 with ramp time as the independent variable, rather than the full period.

The significant SEM observations made on the surfaces of specimens tested in the autoclave with different loading conditions are summarized in the micrographs of Fig. 19. The failure process for all four test conditions is transgranular, with fatigue striations and extensive secondary cracking clearly visible in the high ΔK region. These features are roughly the same as those seen in the air tests, pointing, therefore, to the absence of a corrosion fatigue mechanism in these tests. This observation is consistent with the corresponding fatigue data for which the basic trends were closer to ASME Section XI air line.

In Fig. 20 are shown typical micrographs of the fracture surface of a specimen tested in the autoclave with a sinusoidal loading form (R2-5) with a frequency of 17 mHz. The failure mode of this specimen is somewhat different than those observed on the other fracture surfaces. The basic failure process is transgranular with fatigue striations superposed on the quasi-cleavage facets. The degree of secondary cracking is less in specimen than in the specimens tested in air (Fig. 14). Thus the fractographic features of the sinewave test in the autoclave reveal a mixed picture concerning the presence or the absence of corrosion fatigue.

The features show quasi-cleavage facets that are normally associated with an environment-assisted cracking but they also show fatigue striations normally associated with fatigue failure that does not involve the environment. On the other hand, the crack growth data were accelerated with respect to the air line and this has been taken to indicate the presence of a corrosion fatigue mechanism.

The fractographic observations are summarized in the following Table 4, which is constructed in a manner similar to Table 2. The reader may note that for specimens on which cleavage and intergranular fracture were observed, the growth rates fell into the high category. Since these features are characteristic of hydrogen assisted fracture, this observation lends support to a mechanism of hydrogen embrittlement assisted fatigue crack growth.

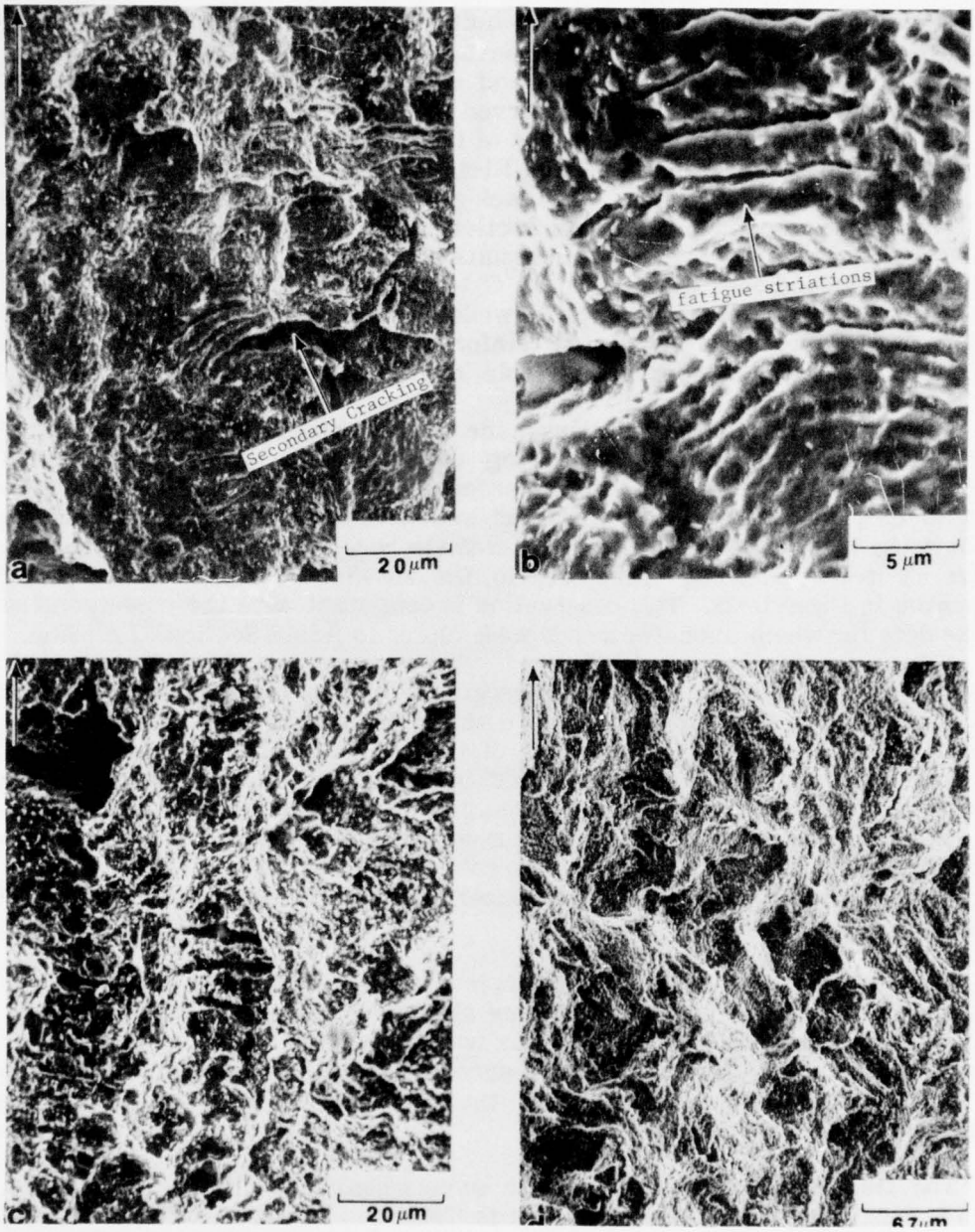

Fig. 19 Fracture surfaces of A508-2 steel tested in the autoclave (288°C, 550°F) with different loading waveforms: (a) and (c) specimen FW-13, (b) and (d) specimen FW-12. The SEM micrographs were taken at crack lengths that correspond to the following values of ΔK: (a) 56 MPa$\sqrt{m}$ (51 ksi$\sqrt{in.}$), (b) 51.2 MPa$\sqrt{in.}$ (52 ksi$\sqrt{in.}$), (c) 50.6 MPa$\sqrt{m}$ (46 ksi$\sqrt{in.}$), and (d) 33 MPa$\sqrt{m}$ (30 ksi$\sqrt{in.}$). The arrows show direction of macroscopic crack propagation. Failure mode for these autoclave tests was transgranular with fatigue striations and extensive secondary cracking. That is, these features are similar to those observed in the air tests that were assumed to represent the baseline fatigue properties.

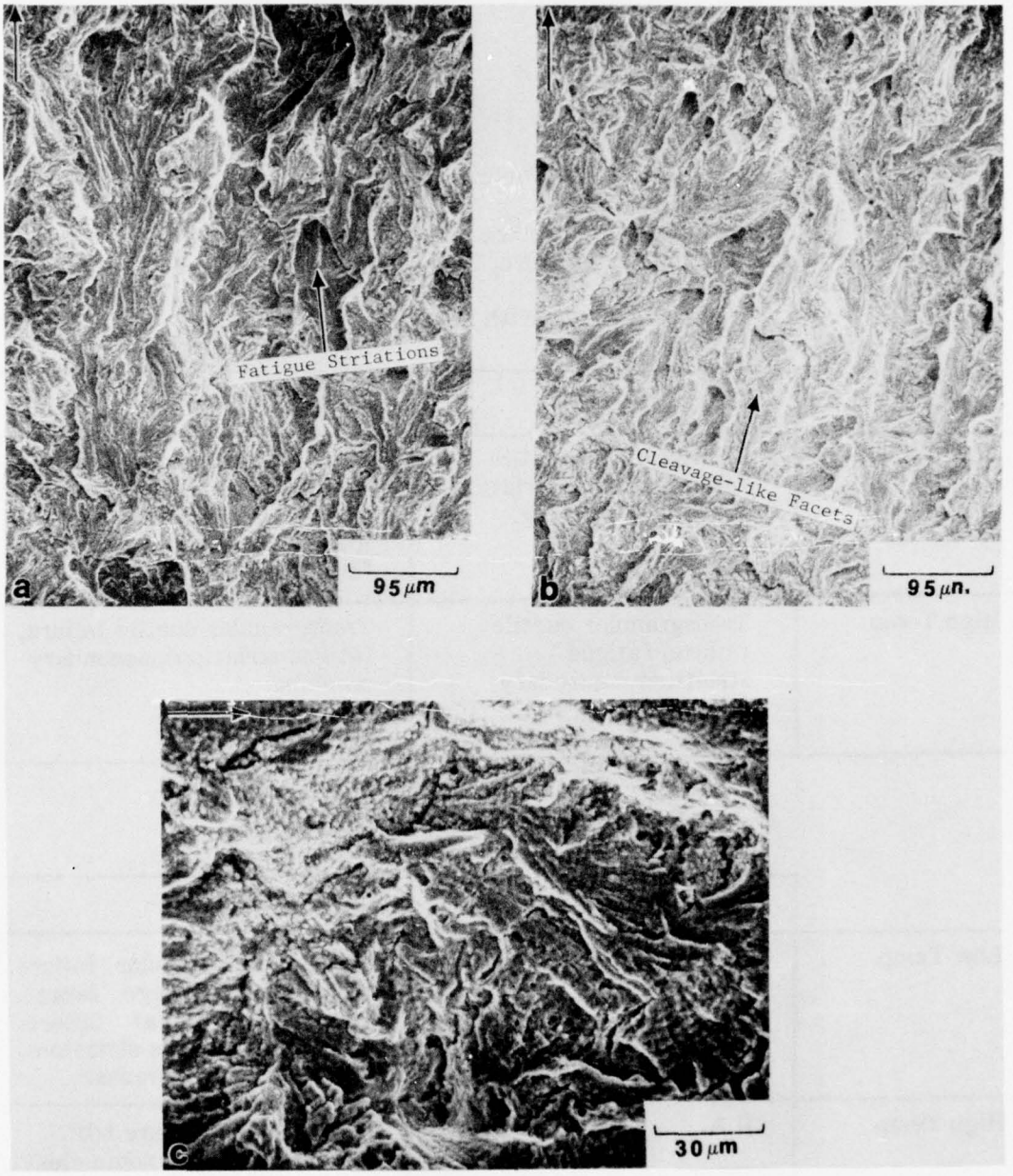

Fig. 20 Fracture surfaces of A508-2 fatigue specimens tested in the autoclave (288°C, 550°F) with a sinusoidal loading (R2-5). The SEM micrographs were taken at crack lengths that correspond to the following values of ΔK: (a) 49.5 MPa$\sqrt{\text{in.}}$ (45 ksi$\sqrt{\text{in.}}$), (b) 55 MPa$\sqrt{\text{m}}$ (50 ksi$\sqrt{\text{in.}}$) and (c) 57.2 MPa$\sqrt{\text{m}}$ (52 ksi$\sqrt{\text{in.}}$). Arrows show direction of macroscopic crack propagation. The predominant failure mode is transgranular with fatigue striations. However, some areas of the fracture surfaces show cleavage-like facets; the degree of secondary cracking was less in this specimen than in the specimen tested in air.

Table 4

Summary of Fatigue Fracture Surface Characteristics as Functions of Temperature, Rise Time and Hold Time

Table 4a Tests With Long Hold Times

	Short Rise Time	Long Rise Time
Low Temp	Transgranular ductile failure, fatigue striations secondary cracking.	Mostly transgranular failure with quasi-cleavage facets, some intergranular failure. Absence of fatigue striations, fewer secondary cracks.
High Temp	Transgranular ductile failure, fatigue striations, secondary cracking.	Transgranular ductile failure, fatigue striations, secondary cracking.

Table 4b Tests with No Hold Time

	Short Rise Time	Long Rise Time
Low Temp	N.A.	Mostly transgranular failure with quasi-cleavage facets, some intergranular failure. Absence of fatigue striations, fewer secondary cracks.
High Temp	N.A.	Transgranular failure with fatigue striations, some cleavage-like facets, fewer secondary cracks.

A MODEL FOR HYDROGEN ASSISTED FATIGUE CRACK GROWTH

The enhanced cyclic crack growth rate seen in previous investigations in reactor grade water as well as in other aqueous environments is most often suggested to be due to hydrogen assisted cracking [5, 19-25]. Other mechanisms have been considered, also, especially in connection with the temperature and frequency dependence of the crack growth rate. For instance, it has been suggested that, in addition to hydrogen, anodic dissolution may induce an increase in crack growth rate [24] or, on the contrary, introduce crack blunting with low frequencies, or during hold times, resulting in subsequent crack growth retardation [13, 14, 26]. At higher temperatures, i.e., closer to the reactor operating temperatures, the formation of a more stable oxide layer may prevent hydrogen absorption [26]. Finally, dynamic strain aging may occur at operating temperatures, resulting also in crack growth retardation. [27-29]

Hydrogen Generation at the Crack Tip

In aqueous environments, the electrochemical conditions at the crack tip during both sustained and cyclic loading have been shown to be independent of the bulk electrochemistry. Under a free corrosion potential, the pH is found to be close to 3.5 [19, 30, 31], i.e., the condition is acidic, and is accompanied by hydrogen evolution through a cathodic reaction. During the rise time of the fatigue cycle fresh metal surface at the advancing crack tip is exposed to this environment. Subsequently, hydrogen generated during the cathodic reaction and hydrolysis can enter the metal. If a hold time is included in the loading wave form, a rapid passivation may occur and subsequent hydrogen entry can be prevented.

Two different theories on the hydrogen concentration profile around the crack tip have been presented. It has been postulated [see e.g. Refs 32-35] that hydrogen diffuses by bulk diffusion to the highest hydrostatic stress state in the plastic zone ahead of the crack tip. Using the formula, $\delta = 2r = K^2/\sigma E$ (proposed by Rice [36]), the distance r of the highest hydrostatic stress state near the crack tip varies from about 0.1 μm for the starting K_{min} to about 200 μm for the K_{max} at the end of the test. The bulk diffusion rate of hydrogen is so low that within a few seconds at ambient temperatures it allows an excess concentration of hydrogen to be accumulated only at distances of a few micrometers [36, 37]. Hydrogen bulk diffusion is 1 to 2 orders of magnitude higher in the temperature range of 93 to 288°C than it is at ambient temperature. This allows for greater hydrogen penetration both at 93 and 288°C.

Another approach, which allows substantially larger diffusion distances, is the dislocation sweep-in mechanism [37, 38]. According to this model mobile dislocations transport hydrogen as Cottrell atmospheres at a rate appreciably in excess of that for lattice diffusion. Thus an excess concentration of hydrogen can be generated throughout the plastic zone.

The presence of hydrogen in the plastic enclave introduces a macroscopic embrittling effect and subsequent increase in cyclic crack growth rate. Considering the basic mechanisms of the microscopic hydrogen effects [see reviews Refs 39-42], a great controversy is, however, apparent. In his recent review Thompson concludes that hydrogen can affect fracture when its concentration in a certain volume reaches a critical level and that all the fracture modes can be affected.

At the present time no preference to the various models can be given. The following text presents some proposed mechanisms, which appear to be relevant when considering the explanation of the observed behaviorism. It has been shown that hydrogen impedes the dislocation motion, i.e., increases the flow stress in the plastic zone [39-43]. This in turn results in a smaller plastic zone size [44-45] and in a lower crack closure load, i.e. larger effective ΔK (at least in the lower ΔK region); these, in turn, resulting in an accelerated crack growth rate [46, 47]. On the other hand, Beachem [33, 48] has suggested a contradictory model according to which hydrogen reduces the local stress required for dislocation motion. Also, Hirth and Johnson [39] have stated that in the case of void coalescence and a fixed plastic zone size such a lower local yield stress would indeed give a lower stress intensity for crack propagation.

Another approach, based on continuum mechanics models, states that a delicate balance exists at a crack tip between cleavage and plastic deformation in ferritic iron alloys [49-51]. Hydrogen may, by forming surface hydrides [49-50], or by lowering the surface energy [52], or the cohesive energy [53-56] suppress plastic deformation and hence favor cleavage fracture.

Hydrogen Embrittlement Mechanism at 93°C

The results presented earlier show that a waveform composed of a fast rise time (of the order of 1 second) followed by a hold time does not accelerate the crack growth rate significantly above the ASME Section XI air line (see Fig. 4). This result is consistent with several previous results obtained in different aqueous environments using various wave forms and frequencies faster than or of the order of one sec [5, 13, 21, 22, 57-60, 13a, 58, 59]. However, an exception is the data published by Atkinson and Lindley [25] which show accelerated crack growth rates even with 1 Hz frequency.

The explanation for the general absence of environmental effect at such comparatively high frequencies may be sought from the passivation behavior of the fresh metal surface at the crack tip and subsequent possibilities of hydrogen absorption and transport. Using a constant strain rate stress corrosion cracking test method, it has been shown that a maximum attack of the environment is observed over a critical range, and the susceptibility decreases at faster and slower strain rates [61-63].

For a corrosion fatigue test at high frequencies, corresponding to larger strain rates in constant strain rate testing, the interaction of the exposed metal with the environment is of no consequence, because the rate at which the metal

fails by ductile fracture exceeds the rate at which the environment can affect fracture via any of the possible mechanisms (dissolution, hydrogen embrittlement or adsorption of damaging species).

Because there is opportunity for hydrogen generation and subsequent entry into the metal, a long rise time, with or without a hold time, produces an accelerated growth rate. The passivation at the frequencies used is not rapid enough to prevent the hydrogen entry. The change of $da/dN - \Delta K$ slope at higher crack growth rates (i.e., the bending of the curve towards the air line (see Fig 6a, b)) can be explained by considering the hydrogen transportation. It has been shown that the amount of hydrogen transported per unit strain decreases with increasing strain rate [64] in agreement with the constant strain rate test results. Also, with the increased surface area generated during the higher crack growth rate the electrochemical conditions change the potential, causing a more anodic state [30], with the consequence that the level of surface hydrogen release decreases [65]. Thus, at higher ΔK values the crack growth rate is so fast that it overcomes the hydrogen generation and transportation [8].

The preceding fractographic observations show that the fracture mode of specimens that produced accelerated growth rates was a quasi-cleavage type transgranular fracture with occasional intergranular areas. Even in the higher ΔK regions, fatigue striations were not observed. These observations support the hydrogen effect, however, no distinction can be made as to the exact mechanisms. The cleavage type fracture is consistent with all the suggested models. The intergranular fracturing, however, would give support to the hydrogen transport by dislocation sweep-in model. The dislocations can move the hydrogen to the grain boundaries, where it is trapped and consequently introduces an intergranular failure when the boundary is favorably oriented with respect to the crack plane.

The fractography of specimens showing an unaccelerated growth revealed a transgranular ductile fracture with fatigue striations. This evidently shows the absence of hydrogen or other environmentally effected embrittlement.

The metallography of the specimens showing accelerated crack growth rates revealed, in the region close to the crack, small holes or voids, as well as the separation of the inclusions from the matrix. Only a very few voids could be seen in specimens showing non-accelerated crack growth rates. This strongly supports the mechanism of hydrogen diffusion ahead of the crack tip and at least partial trapping to the inclusions. This trapping obviously causes reduction in the bond strength at the interface between the inclusions and the matrix, resulting in crack growth preferentially through the inclusions.

Another significant observation was the almost complete absence of microcracks in the specimens showing accelerated crack growth rates. This is apparently due to the hydrogen induced change in fracture mode from ductile striation formation to quasi-cleavage. It is obvious that in the absence of the microbranching, the effective ΔK is higher and consequently the crack growth rates faster. At higher K-values, when the crack growth rate exceeds the hydrogen diffusion rate, the amount of microcracking increases and introduces a reduction in the crack growth rate, i.e., a bend-over (Fig. 6b).

Embrittlement Mechanisms at 288°C

As was the case at 93°C, high frequencies i.e., short rise times of the order of one sec, did not exhibit the accelerating effect of the environment. At NRL no high temperature tests have so far been completed with long rise time, no hold time, and fast reset. However, if the sine wave loading is assumed to closely represent this type of loading, it is obvious that an accelerated crack growth is seen at least for the mid-range ΔK values. This behavior may be explained using the reasoning as in the case of data observed at 93°C, i.e., hydrogen is generated and adsorbed or absorbed during the long rise, subsequently introducing the embrittling effect and accelerated crack growth rate.

Contrary to the observations at 93°C, a hold time, after long rise, depresses the crack growth rate back to the air line. Several mechanisms may be suggested to explain this temperature dependent behavior. It could be assumed that a hydrogen redistribution and accompanying stress relaxation occurs at this temperature. Dislocations moving to the crack tip during relaxation may sweep the hydrogen out of the material, resulting in additional relaxation. It is obvious that a similar relaxation is not possible at lower temperatures, i.e., the crack tip remains sharper during hold times at 93°C. Secondly, it has been postulated that anodic dissolution occuring during hold time or at very low frequencies may introduce excessive crack blunting [13, 14, 25]. Why this blunting should occur at 288°C but not at 93°C is, difficult however, to explain. Thirdly, some kind of stable oxide formation may occur reducing the subsequent hydrogen generation and entry during the following rise time [13]. The oxide formed at 288°C is known to be more stable than that formed at 93°C [66]. Fourthly, if surface hydrogen formation has occurred during the rise time, this hydride may dissolve during the hold time. Lastly, a dynamic strain aging may occur during the hold time resulting in an increased toughness and thus decreased crack growth rate [27-29]. No preference can be given to any of the above mechanisms; it is also possible that several of the suggested processes may occur simultaneously.

The evident discrepancy between the sine wave results (Fig. 6b) and the 1 min ramp and 1 min reset transgranular waveform (Fig. 7) is rather difficult to explain. A possible explanation may be that the crack growth rate achieves a maximum at a certain frequency, which might be of the order of 17 mHz. The triangular wave form result may represent the case for which the reset time is long enough for one or more of the above mechanisms to occur. Another possibility may be that during the reset, the dislocations pump the hydrogen out. There is an evident need for the additional tests to solve the discrepancy. The fractography performed on the non-accelerated specimens tested at 288°C showed only ductile transgranular fracture with fatigue striations, i.e., no evidence of environmental effect. In sinewave specimens giving accelerated crack growth rate, a superposed pattern of quasi-cleavage and fatigue striations was seen. However, it has been previously shown that the fracture mode of hydrogen assisted cracking transforms from mixed inter- and transgranular at lower temperatures (close to 100°C) to fully transgranular at higher temperatures (close to 300°C) [67, 68], and that hydrogen may also assist fracturing in the predominantly ductile manner [41].

Both the air tests reported here showed crack growth rates in the "low" category, near the ASME Section XI air default line. It has been shown that moist air at lower temperatures may cause accelerated crack growth rate [45]. However, in a test conducted at 288°C it is highly unlikely that any moisture can exist close to the heated specimen surface. A need for additional air test with either 17 mHz cpm wave or 1 min ramp/fast reset loading is evident.

CONCLUSIONS

There are several observations, conclusions, and suggested mechanistic processes which have evolved from these studies. While each of these has been stated and developed in the foregoing sections on results, mechanisms and fractography, they are summarized here for conciseness and mental digestive ease.

1. Crack growth rates for these load ratio (0.1), temperature (93 and 288°C, 200 and 550°F) and waveform (ramp and hold) conditions fall either in a band situated near the Section XI air default line ("low"), or midway between the air and water default lines ("high").

    a. A ramp time in excess of one sec. is required in order to produce data in the high category.

    b. In spite of a long ramp time, a high temperature test involving a hold time component as well, will result in crack growth rates in the low category.

2. For the test parameters of this study, crack growth rates did not exceed the ASME Section XI code limit for the high-temperature, pressurized water environment. However, it is clear from other references that certain conditions, such as high load ratios (~0.7 [5]) or boiling water reactor water chemistries (~100 ppb dissolved oxygen), together with a high load ratio (0.6 [69]) result in fatigue crack growth rates which exceed ASME Code limits.

3. The two waveforms which provided the highest crack growth rates are the 17 mHz sinewave and the one min ramp/fast reset waveforms. These two waveforms have been chosen for the main matrix test program.

4. To account for these observations, a hydrogen embrittlement mechanism has been advanced. The primary elements of this model are:

    a. As fresh metal surface is exposed during the ramp time of a load waveform, the hydrolytic reaction results in the generation of hydrogen which subsequently diffuses to the region of highest triaxial stress. Repassivation rates are not high enough to prevent continued hydrogen entry.

    b. At low temperatures, stress relaxation and diffusion of hydrogen from the plastic enclave is not possible, and the crack

growth rates remain high even with the presence of hold time components in the waveform.

c. At high temperatures, either stress relaxation, crack tip blunting, stable oxide passivation or dynamic strain aging, or a combination of these, results in the depression of expected high crack growth rates to the low growth rate category.

5. In large measure, the basis for these mechanistic processes is found in the fractographic evidence.

a. Transgranular cleavage, some intergranular separation, and an absence of fatigue striations characterize the fatigue fracture surfaces of the low temperature, high growth rate specimens. This is characteristic of a hydrogen assisted cracking mechanism.

b. High or low temperature fatigue fracture surface morphology for the low growth rate specimens is typified by ductile fracture with fatigue striations. This implies the lack of a hydrogen assistance.

c. High temperature, high growth rate (sinewave) fatigue fracture surface morphology consisted of a superposed pattern of quasi-cleavage and fatigue striations. This is consistent with higher temperature hydrogen assisted growth mechanisms.

IMPLICATIONS OF THESE RESULTS FOR ASME SECTION XI.

In each of the Figs. 4-6 the ASME Section XI Code default lines for surface and subsurface flaws are illustrated. An immediate conclusion is that for the material, load waveform and environmental combinations used in this study, the code line for surface flaw growth has been acceptably (conservatively) chosen. It is most important to note that the load ratio for this study was ~0.1 and there is ample evidence [5,6] that higher load ratios (0.5, 0.7) will result in higher growth rates which exceed the code limitations. NRL studies of growth rates as a function of higher load ratios are underway, but it is clear that this lower load ratio results in acceptably low growth rates irrespective of temperature and waveform.

It is also important to note that the bend-over of the sinewave generated growth rates is peculiar only to that waveform. The data pertaining to the ramp/hold waveforms do not bend over and in fact tend to reside in bands nearly parallel to the current ASME code limits. This strongly supports the contention that the code limit lines should remain linear and unsegmented. Again, this conclusion can only be held valid for the conditions (especially the load ratio = 0.1) of this series of tests.

Lastly, it must be remembered that the limited number of waveform constructions, and the two temperatures used in this work, were not meant to

completely span the range of operating reactor conditions. However, the execution of this preliminary matrix, and the main matrix on which work has just begun has been a major stride forward in the accurate measurement of fatigue crack growth rates in the high-temperature pressurized reactor-grade water environment. Thus, the data base on which the ASME Sec. XI Code is based has been further strengthened.

ACKNOWLEDGEMENTS

The investigations reported were sponsored by the Reactor Safety Research Division of the Nuclear Regulatory Commission. The continuing support of this agency is appreciated.

The litany of individuals who contributed heavily to this effort, but who are not included in the authorship, is long. While page-long acknowledgements in outside publications are discouraged, an NRL produced document such as this seems to be the ideal place to thank each of these people. Mr. Lendell Steele, Head of the Thermostructural Materials Branch, must be thanked for his encouragement and support of the group as a whole. One of the authors, Dr. Frank J. Loss, has consistently sought the highest scientific standards for this group and has been responsible for the on-going sponsor-NRL liaison.

There are many members of the supporting staff at the NRL whose careful work has offered significant progress and improvements to our fatigue crack growth facility. The chief technician on this project, Mr. Robert E. Taylor, has repeatedly demonstrated his mechanical ingenuity, and much of the success of this work is a direct result of his development of, or rapid comprehension, of the techniques involved in this type of experimental work. Mr. Carroll Garland performed much of the machining of specimens, fixtures and auxiliary equipment. Mr. William Hagel assisted with his very careful and expeditious electrical expertise. Mr. John Forsyth designed and constructed the water circulation loops and hydraulic control loop of the 2/4T autoclave.

Within our group at the NRL, we strongly encourage the employment of college students on either co-operative work/education or junior fellowship programs. In return for their often enthusiastic and careful assistance with the day-to-day operation of the fatigue crack growth facility, these students are placed in a learning environment, quite unlike the academic environment, which will serve them very well in their ensuing careers. Over the past three years of this particular research effort, Ross Iwamoto, William Baracat, Michael Fitzpatrick and Loren Garroway have been of invaluable assistance to this program.

Because of the high visibility of the Thermostructural Materials Branch, and the high-temperature pressurized water fatigue crack growth work in particular, a number of laboratories in foreign countries have sponsored extended appointment of their employees to our group here at the NRL. These individuals share their expertise with us while they study our developing techniques in this area of research. Dr. Dietmar Sturm, Materialprufungsanstalt, Stuttgart, Germany, and Ms. Giovanna Gabetta-Zanotti, Centro Informazioni Studi Esperienze, (CISE), Milano, Italy have both assumed responsible and highly interactive

residencies in our group. A third scientist, Dr. Kari Torronen, Technical Research Centre of Finland, has made a major contribution to this paper, in the area of mechanistic studies of fatigue crack growth, and is included among the authors.

REFERENCES

1. W.H. Bamford, et al, "Effect of High-Temperature, Primary Reactor Water on the Fatigue Crack Growth of Reactor Vessel Steels" in *HSST* Quarterly Progress Report for April-June 1977, ORNL/NUREG/7M-147, pp. 16-28, (Dec 1977).

2. W.H. Cullen, et al, "A Computerized Data Acquisition System for a High-Temperature, Pressurized Water Fatigue Test Facility" in Computer Automation of Materials Testing, a forthcoming STP, American Society for Testing and Materials, Philadelphia, PA 19103.

3. D.K. Sturm, F.J. Loss and W.H. Cullen, "Qualification of Crack Growth Data Beyond ASTM Committee E-24 Criteria," Report of NRL Progress, pp. 4-9 (Sept. 1978)pp 4-9.

4. L.A. James, "Specimen Size Considerations in Fatigue-Crack Growth Rate Testing", HEDL-TME 78-99, Hanford Engineering Development Laboratory, P.O. Box 1970, Richland, WA 99352

5. W.H. Bamford and D.M. Moon,"Some Mechanistic Observations on the Crack Growth Characteristics of Pressure Vessel and Piping Steels in PWR Environment" Corrosion 79, Atlanta, GA, National Association of Corrosion Engineers (1979).

6. W.H. Bamford, D.M. Moon, and L.J. Ceschini, "Effect of High-Temperature Primary Reactor Water on the Subcritical Crack Growth of Reactor Vessel Steels" in HSST Quarterly Progress Report for October-December, 1977, ORNL/NUREG/TM-194, pp. 25-35, (May 1978).

7. W.H. Bamford and L.J. Ceschini, "Effects of High Temperature Primary Water on the Fatigue Crack Growth of Reactor Vessel Steels" in HSST Quarterly Progress Report for July-September, 1977, ORNL/NUREG/TM-166 pp. 38-45, (April 1978).

8. W.H. Bamford, D.M. Moon, and L.J. Ceschini, "Effects of High Temperature Primary Water on the Fatigue Crack Growth of Reactor Vessel Steels" in HSST Quarterly Progress Report, ORNL-NUREG/TM-239, pp. 9-18, (Oct. 1978).

9. W.H. Bamford, D.M. Moon & L.J. Ceschini, "Effects of High Temperature Primary Water on the Fatigue Crack Growth in Reactor Vessel Steels" in HSST Quarterly Progress Report for July-September, 1977, ORNL/NUREG/TM-275, pp. 21-29 (January 1979).

10. W.H. Bamford, D.M. Moon and L.J. Ceschini, "Effects of High Temperature Primary Water on the Fatigue Crack Growth of Reactor Vessel Steels" in HSST Quarterly Progress Report, ORNL/NUREG/TM-298, pp. 14-23, April (1979).

11. W.H. Cullen et al, "Evaluation of Starting ΔK Phenomenon on Cyclic Crack Growth in A508 Pressure Vessel Steels", Report of NRL Progress, pp. 14-17 (July 1978).

12. J.A. Knight, "Corrosion Fatigue of Welded, Quenched and Tempered Steels," Welding Research International, 7(5), pp. 17-39 (1978).

13. T. Kondo, et al, "Fatigue Crack Propagation Behaviour of ASTM A533B and A302B Steels in High Temperature Aqueous Environment," Paper No. 6, HSST Program, Sixth Annual Information Meeting, April 1972.

14. M. Suzuki et al, "The Environment Enhanced Crack Growth Effects in Structural Steels for Water Cooled Nuclear Reactors" Paper C125/77 in Proceedings, Institute of Mechanical Engineers, London, pp. 161-169, (1977).

15. P.H. Hutton, E.B. Schwenk and R.J. Kurtz, "Acoustic Emission - Flaw Relationship for In-Service Monitoring of Nuclear Pressure Vessels," in Quarterly Report of Reactor Safety Research Programs, NUREG/CR-0341, Pacific Northwest Laboratory, Richland, WA, p. 17-61 (1978).

16. H.E. Watson, B.H. Menke, and F.J. Loss in "Structural Integrity of Water Reactor Pressure Boundary Components, Progress Report Ending 28 February 1977" NRL Memo Report 3512, (May 1977).

17. C. Laird, "The Influence of Metallurgical Structure on the Mechanisms of Fatigue Crack Propagation," ASTM Conf. on Fatigue Crack Propagation, Atlantic City, 1966, ASTM Spec. Tech. Publ. 415, Philadelphia, 1967, pp. 131-168.

18. V. Provenzano and F.A. Smidt, Jr., in "Structural Integrity of Water Reactor Pressure Boundary Components; Progress Report Ending 31 May 1977" NRL Memo Report 3600, (Sept. 1977)

19. J.P. Gallagher, "Corrosion Fatigue Crack Growth Rate Behavior Above and Below K_{ISCC} in Steels," Journal of Materials, 6, pp. 941-964 (1971). (Also Naval Research Laboratory Report No. 7064, Washington, DC, (May 28, 1970).

20. J.M. Barsom, "Mechanisms of Corrosion Fatigue Below K_{ISCC}," Inst. J. Fracture Mech., 7, pp. 163-182 (1971).

21. J.M. Barsom, "Effect of Cyclic Stress Form on Corrosion Fatigue Crack Propagation Below K_{ISCC} in a High Yield Strength Steel," in Corrosion Fatigue: Chemistry Mechanics and Microstructure, NACE-2, eds. O. Devereux et al, National Association of Corrosion Engineers, Houston, TX 77027, pp. 424-436 (1973).

22. T.R. Mager, J.D. Landes, D.M. Moon and V.J. McLaughlin, "The Effect of Low Frequencies on the Fatigue Crack Growth Charactersitics of A533 Grade B Class 1 Plate in an Environment of High-Temperature Primary Grade Nuclear Reactor Water", Heavy Sections Steel Technology Technical Report No. 35, WCAP-8256, Westinghouse Electric Corporation, Pittsburgh, PA, (Dec 1973).

23. T.R. Mager, D.M. Moon and J.D. Landes, "Fatigue Crack Growth Character istics of A533 Grade B Class 1 Plate in an Environment of High-Temperature Primary Grade Nuclear Reactor Water," Trans. ASME Ser. J, J. Pressure Vessel Technical, 99, pp. 238-247 (1977).

24. O. Vosikovsky, "Fatigue-Crack Growth in an X-65 Line-Pipe Steel at Low Cyclic Frequencies in Aqueous Environments," Trans. ASME, Ser. H., J.Eng. Mat. and Technology, 97, pp. 298-304 (1975).

25. J.D. Atkinson and T.C. Lindley, "The Effect of Frequency and Temperature on Environmentally Assisted Fatigue Crack Growth Below K_{ISCC} in Steels" in The Influence of Environment on Fatigue, Inst. Mech. Engrs., London pp. 65-74 (1977).

26. J.C. Radon, C.M. Branco and L.E. Culver, "Crack Blunting and Arrest in Corrosion Fatigue of Mild Steel", Int. Journ. of Fracture, 12, pp. 467-469 (1976).

27. K. Kussmaul, R. Schafer and D. Blind, "The Effect of Fatigue Embrittlement on Crack Growth and Fracture Behaviour," in Time and Load Dependent Degradation of Pressure Boundary Materials, IAEA, Innsbruck (1978).

28. C.E. Richards and T.C. Lindley, "The Influence of Stress Intensity and Microstructure on Fatigue Crack Propagation in Ferritic Materials", Engrg. Fracture Mech., 4, pp. 951-978 (1972).

29. M. Hirose, N. Hasegawa and Y. Kato, "Effect of Cyclic Strain Aging on the Critical Cyclic Stress Required to Propagate a Crack in Low Carbon Steels," Bulletin of JSME, 21, pp. 1201-1207 (1978).

30. B.F. Brown, C.T. Fujii, and E.P. Dahlberg, "Methods for Studying the Solution Chemistry Within Stress Corrosion Cracks", J. Electrochem. Soc., 116, pp. 218-219 (1969).

31. J.A. Smith, M.H. Peterson and B.F. Brown, "Electrochemical Conditions at the Tip of an Advancing Stress Corrosion Crack in AISI 4340 Steel," Corrosion, 26, pp. 539-542 (1970).

32. A.R. Troiano, "The Role of Hydrogen and Other Interstitials in the Mechanical Behavior of Metals," Trans. ASM, 52, pp. 54-80 (1960).

33. C.D. Beachem, "A New Model for Hydrogen Assisted Cracking," Met. Trans., 3, pp. 437-451 (1972)

34. W.W. Gerberich, "Effect of Hydrogen on High-Strength and Martensitic Steels", in Hydrogen in Metals, eds. I.M. Berstein and A.W. Thompson, American Society for Metals, Metals Park, OH 44073, pp. 115-147 (1974).

35. W.W. Gerberich, J. Garry, and J.F. Lessar, "Grain Size and Concentration Effects in Internal and External Hydrogen Embrittlement," in Effect of Hydrogen on Behavior of Materials, eds. A.W. Thompson and I.M. Bernstein, Metallurgical Society of AIME, New York, NY 10017, pp. 70-82 (1976).

36. J.R. Rice, "Mechanics Aspects of Stress Corrosion Cracking and Hydrogen Embrittlement," in Stress Corrosion Cracking and Hydrogen Embrittlement of Iron Base Alloys, NACE-5, eds. R.W. Staehle et al, National Association of Corrosion Engineers, Houston, TX 77027, pp. 11-15 (1977).

37. J.K. Tien, R.J. Richards, O. Buck and H.L. Marcus, "Model of Dislocation Sweep-In of Hydrogen During Fatigue Crack Growth", Scripta Met., 9, pp. 1097-1101 (1975).

38. J.K. Tien, A.W. Thompson, I.M. Bernstein and R.J. Richards, "Hydrogen Transport by Dislocations," Met. Trans A, 7A, pp. 821-829 (1976).

39. J.P. Hirth and H.H. Johnson, "Hydrogen Problems in Energy Related Technology," Corrosion, 32, pp. 3-15 (1976).

40. E.N. Pugh, "A Post Conference Evaluation of Our Understanding of the Failure Mechanics," in Stress Corrosion Cracking and Hydrogen Embrittlement of Iron Base Alloys, NACE-5, eds. R.W. Staehle et al, National Association of Corrosion Engineers, Houston, TX 77027, pp. 37-51 (1977).

41. A.W. Thompson, "Microstructural Factors in Hydrogen Embrittlement and Stress Corrosion Cracking," in Environmental Degradation of Engineering Materials, eds. M.R. Louthan and R.P. McNitt, Virginia Tech., Blacksburg, VA, p. 13-17 (1977).

42. M. Cornet and S. Talbot-Besnard, "Present Ideas About Mechanisms of Hydrogen Embrittlement of Iron and Ferrous Alloys," Met. Sci., 12, pp. 335-339 (1978).

43. M.R. Louthan, G.R. Caskey, J.A. Donovan and D.E. Rawl, "Hydrogen Embrittlement of Metals," Material Science Engineering, 10, pp. 357-368 (1972).

44. J.D. Frandsen and H.L. Marcus, "The Correlation Between Grain Size and Plastic Zone Size for Environmental Hydrogen Assisted Fatigue Crack Propagation," Scripta Met., 9, pp. 1089-1094 (1975).

45. D.L. Davidson and J. Lankford, "The Influence of Water Vapour on Fatigue Crack Plasticity in Low Carbon Steel" in Fracture 1977, ed. D.M.R. Taplin, ICF4, Waterloo, p. 897-904 (1977).

46. W.L. Morris, J.D. Frandsen and H.L. Marcus, "Environmentally Induced Transitions in Fatigue Fracture Mode," in Fractography - Microscopic Cracking Processes, STP 600, eds. C.D. Beachem and W.R. Warke, American Society for Testing and Materials, Philadelphia, PA 19103, pp. 49-61 (1976).

47. A.J. McEvily, "Current Aspects of Fatigue," Metal Sci., 11, pp. 274-284 (1977).

48. C.D. Beachem, "Electron Fractographic Support for a New Model for Hydrogen-Assisted Cracking," in Stress Corrosion Cracking and Hydrogen Embrittlement of Iron Base Alloys, NACE-5, eds. R.W. Staehle et al, National Association of Corrosion Engineers, Houston, TX 77027, pp. 376-389 (1977).

49. J.J. Gilman, "Stress-Corrosion Cracking in Plastic Solids Including the Role of Hydrogen," Phil. Mag., 26, pp. 801-812 (1972).

50. J.J. Gilman, "The Role of Surface Hydrides in Stress-Corrosion Cracking," in Stress Corrosion Cracking and Hydrogen Embrittlement of Iron Base Alloys, NACE-5, eds. R.W. Staehle et al, National Association of Corrosion Engineers, Houston, TX 77027, pp. 326-331 (1977).

51. J.R. Rice and R. Thomson, "Ductile versus Brittle Behaviour of Crystals," Phil. Mag., 29, pp. 73-97 (1974).

52. R. Thomson, "Brittle Fracture in a Ductile Material with Application to Hydrogen Embrittlement," J. Mater. Sci., 13, pp. 128-142 (1978).

53. R.A. Oriani, "A Mechanistic Theory of Hydrogen Embrittlement of Steels," Berichte der Bunsen-Gesellschaft, 76, pp. 848-857 (1972).

54. R.A. Oriani, "A Decohesion Theory for Hydrogen-Induced Crack Propagation," in Stress Corrosion Cracking and Hydrogen Embrittlement of Iron Base Alloys, NACE-5 eds. R.W. Staehle et al, National Association of Corrosion Engineers, Houston, TX 77027 (1977).

55. R.A. Oriani and P.H. Josephic, "Equilibrium Aspects of Hydrogen-Induced Cracking of Steels," Acta Met., 22, p. 1065-1074 (1974).

56. R.A. Oriani and P.H. Josephic, "Equilibrium and Kinetics Studies of the Hydrogen-Assisted Cracking of Steel," Acta Met., 25, p. 979-988 (1977).

57. T.R. Mager and V.J. McLoughlin, "The Effect of an Environment of High Temperature Primary Grade Nuclear Reactor Water on the Fatigue Crack Growth Characteristics of A533 Grade B Class 1 Plate and Weldment Material," Heavy Section Steel Technology Program Technical Report No. 16, WCAP-7776, Westinghouse Electric Corporations, Pittsburgh, PA, (Oct. 1971).

58. T. Kondo, T. Kikuyama, H. Nakajima and M. Shindo, "Fatigue Crack Propagation Behaviour of ASTM A533B and A302B Steels in High Temperature Aqueous Environment," Paper No. 6, Heavy Section Steel Technology Program, 6th Annual Information Meeting, Oak Ridge National Laboratory, Oak Ridge, TN 37830, (Apr. 1972).

59. E. Kiss, T.L. Gerber and J.D. Heald, "Evaluation of Fatigue Crack Growth in a Simulated Light Water Reactor Environment," Closed Loop, 4, pp. 3-9 (Spring 1974).

60. T.L. Gerber, J.D. Heald and E. Kiss, "Fatigue Crack Growth in SA508-C12 Steel in a High Temperature, High Purity Water Environment," Trans. ASME, ser. H, J. Eng. Mat. and Technology, 96, pp. 255-261 (1974).

61. R.N. Parkins, F. Mazza, J.J. Roynela and J.C. Scully, "Stress Corrosion Test Methods. Report prepared for the European Federation of Corrosion Working Party on Stress Corrosion Test Methods," Br. Corros. J., 7, pp. 154-167 (1972).

62. J. Kruger, "New Approaches to the Study of Localized Corrosion," in Passivity and Its Breakdown on Iron and Iron Base Alloys, eds. R.W. Staehle and H. Okada, National Association of Corrosion Engineers, Houston, TX 77027, pp. 35-41 (1976).

63. J.C. Scully, "Mechanism of Dissolution - Controlled Cracking," Metal Sci., 12, pp. 290-300 (1978).

64. M.R. Louthan, "Effects of Hydrogen on the Mechanical Properties of Low Carbon and Austenitic Steels," in Hydrogen in Metals, eds. I.M. Bernstein and A.W. Thompson, American Society for Metals, Metals Park, OH 44073, pp. 53-75 (1974).

65. W.E. Ruther and R.K. Hart, "Influence of Oxygen on High Temperature Aqueous Corrosion of Iron," Corrosion, 19, pp. 127t-133t (1963).

67. R.P. Gangloff and R.P. Wei, "Gaseous Hydrogen Embrittlement of High Strength Steels," Met. Trans. A, 8A, pp. 1043-1053 (1977).

68. R.P. Gangloff and R.P. Wei, "Fractographic Analysis of Gaseous Hydrogen Induced Cracking in 18 Ni Maraging Steel," Fractography in Failure Analysis, STP 645, eds. B.M. Strauss and W.H. Cullen, American Society for Testing and Materials, Philadelphia, PA 19103, pp. 87-106 (1978)

69. D.A. Hale, J.N. Kass, "Fatigue Crack Growth of Low Alloy Steel in a High Temperature, High Purity Oxygenated Water Environment" Paper Number 225, Corrosion/79, Atlanta, GA, National Association of Corrosion Engineers (1979).